Non-contrast Magnetic Resonance Angiography for Evaluation of Peripheral Arterial Disease

Iliyana P Atanasova

Submitted in partial fulfillment of the
requirements for the degree of
Doctor of Philosophy
in the Graduate School of Arts and Sciences

COLUMBIA UNIVERSITY

2013

ABSTRACT

Non-contrast Magnetic Resonance Angiography for Evaluation of Peripheral Arterial Disease

Iliyana P Atanasova

Peripheral arterial disease (PAD) is a major cause of morbidity and mortality in the USA with an estimated prevalence of up to 20% in those over 75 years. Vascular disease and kidney impairment frequently coexist; prevalence of moderate to severe renal dysfunction in PAD patientsis estimated at 27-36%. Knowledge of location, severity, and extent of PAD is imperative for accurate diagnosis and treatment planning. However, all established imaging modalities that are routinely used for treatment planning are contra-indicated in kidney disease patients. Contrast-enhanced x-ray and CT angiography are unsafe due to exposure to nephrotoxic contrast material and ionizing radiation. Recently, the FDA has also warned against the use of gadolinium-enhanced MRA (Gd-MRA) due to evidence that gadolinium could trigger a life-threatening condition known as nephrogenic systemic fibrosis (NSF) in patients with moderate to severe kidney dysfunction. There is a clinical need to develop vascular imaging techniques that are safe in patients with coexisting PAD and renal insufficiency.

The focus of this thesis was the development of a non-contrast alternative to Gd-MRA for imaging of peripheral vessels from renal to pedal arteries. A new imaging sequence for non-contrast visualization of the abdominal and pelvic arteries was designed, implemented, and validated in a small cohort of PAD patients against Gd-MRA. In addition, an existing fast spin-echo based technique for unenhanced imaging of the lower extremities was optimized for improved performance in a clinical setting.

Table of Contents

List of Figures

List of Tables

Acknowledgements

I had met Dr. Andrew Laine only once when he offered to recommend me as a potential PhD student to one of his colleagues, Dr. Vivian Lee. I am grateful for his vote confidence, which in retrospect, offered me an excellent PhD experience both academically and socially. I also thank him for all of his support, while serving as my formal adviser at Columbia.

I am grateful to Dr. Vivian Lee for sponsoring and supervising my PhD workand for giving me a unique perspective to research. I have learned to assess my work in terms of clinical relevance and I find that to be both valuable and personally rewarding. Dr. Lee is also one of the most impressive people I have met. I thought that after getting to know her, I would figure out how she finds the time to be a wife, a mom of four, a hospital CEO, a scientist, and a student all at the same time. Four years later, I still have no clue. Vivian has been and always will be an inspiration to look forward and move forward.

I owe most of the scientific skills that I acquired during my PhD and my understanding of MRI to Dr. PippaStorey. I am grateful for her patience, fantastic lecture slides, and for all the Sunday afternoons we spent together at the scanner console. Thank you for helping me out throughout, especially in the final year when it was completely voluntarily.

The joy Dr. Daniel Kim derives from getting a project to work is contagious. I have been woken up by 7-am text messages (that could have easily waited till 9 am when we met in person) and kept at the scanner past midnight on more than one occasion. I am grateful for his patience and occasional lack thereof, for staying up late, for challenging me every step of the way, and for all the personal advice.

Dr. Ruth Lim has been a reader for all of the clinical studies included in this thesis; she has also proof-read every abstract and every paper that is currently listed on my resume. My PhD

experience would not have been the same without you; thank you for teaching me about anatomy and MRI and for always being ready to help out.

I thank the MRI staff at NYU Radiology and everyone at the CBI who has helped me out throughout the past four years. I am grateful to all the friends and colleagues at NYU and Columbia, particularly my office-mates from room 420 at the CBI, who have shared the pain and the joy of working in research.

Thank you all!

Chapter 1

Introduction

Peripheral arterial disease (PAD) denotes abnormalities of the arteries distal to the aortic arch. The condition, most commonly caused by atherosclerosis [1], presents with vessel narrowing which may lead to obstruction of arterial blood flow and subsequent reduction in tissue perfusion and oxygenation [2-4]. PAD is a major cause of morbidity and mortality in the USA with an estimated prevalence of up to 20% in those over 75 years. Knowledge of location, severity, and extent of the disease is imperative for accurate diagnosis and treatment planning. Digital subtraction angiography (DSA) is the gold standard for assessment of PAD, but in routine clinical practice DSA has been largely replaced by contrast-enhanced computed tomography (CT) or magnetic resonance (MR) angiographic techniques, which are less invasive and safer.

Recently, the Food and Drug Administration (FDA) has warned against the use of gadolinium-enhanced MRA (Gd-MRA) in patients with moderate to severe end-stage renal insufficiency due to evidence that gadolinium could trigger a life-threatening condition known as nephrogenic systemic fibrosis (NSF) in this patient population [5, 6]. Vascular disease and kidney impairment frequently coexist. Prevalence of moderate to severe renal dysfunction in PAD patients is estimated at 27-36% [7]. The main alternative to Gd-MRA, CTA, with its exposure to nephrotoxic contrast material and ionizing radiation is also unsafe for kidney disease patients. Therefore, there exists a clinical need to develop MRA techniques that do not require gadolinium contrast in order to enable safe assessment of vascular conditions in patients with coexisting PAD and renal insufficiency.

Current state-of-the-art moving table Gd-MRA uses a bolus chase approach where 3-4 sequential 3D scans are performed, starting from the abdominopelvic region, then the thighs, and finally the calf and pedal arteries. This work is an attempt to develop a non-contrast alternative to Gd-MRA for comprehensive imaging of the peripheral vessels from the renal to the pedal arteries without the need for gadolinium injection.

In recent years, various new non-contrast techniques have shown promise for evaluation of the abdominal and lower extremity vasculature. Electrocardiographically (ECG)-triggered 3D partial Fourier fast spin echo (ECG-FSE), pioneered by Miyazaki et al [8], is well suited for imaging of slow-flow vascular beds such as the arteries of the calves and thighs. The technique produces venous-free angiograms of the lower extremities by exploiting difference in arterial and venous flow during the cardiac cycle. When technically successful, ECG-FSE MRA accuracy is as high as 90-96% [9-11], even when severe disease is present. However, as currently implemented, ECG-FSE produces non-diagnostic results in as many as 47% of all subjects [10, 12]. Two major factors compromise image quality: (1) image artifacts due to patient motion and (2) differences in flow characteristics between the right and left leg.

Non-contrast techniques for evaluation of the abdominopelvic region have also been reported. Inflow-based MRA with 3D balanced steady-state free precession (b-SSFP) readout and a slice-selective (SS) inversion recovery (IR) pulse has been developed for evaluation of renal arteries [13]. IR b-SSFP MRA is typically performed axially with 100-120 mm craniocaudal coverage, with a single SS-IR pulse applied transversely to overlay completely the imaging slab and to extend inferiorly for venous suppression. Clinical studies report accuracies in the 90-95% range [14-17]; however, the technique is inadequate for comprehensive

assessment of the abdominal and pelvic arteries as the superior-inferior distance between renal arteries and the thighs is on the order of 300 mm.

In this work, we combined ECG-FSE and IR b-SSFP MRA in a 3-station protocol for non-contrast evaluatoin of PAD. ECG-FSE was used for imaging of the calf and thigh regions, while IR b-SSFP was used for the abdominopelvic area. To overcome existing limitations we attempted to (1) extend the coverage of IR b-SSFP by utilizing four preparation pulses and to (2) improve the technical robustness of ECG-FSE by implementing it with two separate sagittal slabs with interleaved systolic and diastolic data acquisition.

The manuscript begins with a brief description of PAD and the clinical tools available for diagnosis and monitoring of the condition (Chapter 2). Next, chapter 3 discusses the physical principles and limitations of existing non-contrast MRA techniques that are suitable for PAD imaging. Chapters 4 and 5 describe the design and validation of a new sequence for unenhanced abdominal MRA. Chapters 6 and 7 focus on a range of experiments aimed at improving the clinical performance of ECG-FSE for imaging of the lower extremities.

Chapter 2

Peripheral Arterial Disease

Peripheral arterial disease (PAD) denotes abnormalities of the arteries distal to the aortic arch. The condition, most commonly caused by atherosclerosis [1], presents with vessel narrowing which may lead to obstruction of arterial blood flow and subsequent reduction in tissue perfusion and oxygenation [2-4]. Early symptoms of PAD, known as intermittent claudication, consist of muscle pain in the legs triggered by exercise and relieved by rest. Further progression of the condition may present with pain at rest. In late stages of the disease, ischemic ulceration and gangrene may be observed due to severe tissue hypoperfusion. This advanced disease state, termed critical limb ischemia, often requires a major amputation and is associated with high 1-year mortality rate [3, 4, 18].

2.1 Epidemiology

Reported incidence and prevalence rates of PAD vary across epidemiologic studies, depending on the methods used to determine presence of disease. According to a 2011 report by the American Heart Association [19], PAD currently affects 8 million people in the USA. Earlier studies state a total prevalence of 27 million people in Europe and North America combined [20]. Among adults older than 55 years, 20% are believed to be affected by PAD. Annual incidence is estimated at 60 new cases per 10 000 people [4].

Primary risk factors for PAD include age, sex, diabetes, and history of smoking. The condition is more common among men and affects primarily elderly individuals. After age 40 the

risk of developing PAD increasing two to three-fold for every 10 year increase in age [4]. Smoking has been found to triple the risk of PAD; initial symptoms of the disease tend to appear 10 years earlier in smokers compared to non-smokers [21-23]. There is a strong link between diabetes and vascular disease. PAD prevalence is found to increase with the duration of diabetes – at10 years after initial diabetes diagnosis, 15% of patients have developed PAD. The percentage increases to 45% at 20 years. Furthermore, PAD progression is faster in diabetic patients leading to higher rates of limb amputations and mortality compared to non-diabetics [21, 24, 25]. Additional risk factors for PAD include hypertension [26], high levels of cholesterol [27], and elevated homocysteine levels which are believed to trigger atherosclerotic processes [28, 29].

2.2 Diagnosis

The first step in diagnosing PAD consists of collecting accurate patient history to rule out non-vascular causes of leg pain [3]. Next, patients undergo ultrasound-based noninvasive vascular laboratory tests, which most commonly consist of measuring ankle brachial index (ABI) and at some clinical sites may additionally include pulse volume recordings, Doppler velocity waveform analysis, or segmental systolic pressure measurements [30]. If these tests are inconclusive or indicate lifestyle limiting disease, patients undergo more extensive imaging tests, including either duplex ultrasound, CT angiography (CTA), or magnetic resonance angiography (MRA), to determine exact location and extent of disease. While the gold standard for PAD evaluation remains DSA, due to its invasiveness, ultrasound, CTA, and MRI are preferred imaging modalities in routine clinical practice nowadays [30, 31].

2.2.1 Ultrasound Imaging and Noninvasive Vascular Laboratory

Ultrasonography is the first-line imaging technique which patients with suspected PAD undergo**.** Two types of echographic techniques are used in PAD evaluation: gray-scale (B-mode) and continuous wave Doppler. The former offers morphological information, while the latter provides quantitative assessment of flow dynamics and vascular functionality. When gray-scaled and Doppler ultrasound are combined in one system, the modality is known as duplex sonography [31].

Doppler ultrasound techniques can visualize blood flow as they are sensitive to frequency shifts in the reflected signal caused by moving targets. Doppler permits to estimate blood flow velocity in vessels because of a known relationship between flow velocity, the frequency of the emitted ultrasound wave, and the frequency of the detected echo. In addition to velocity, Doppler ultrasound also provides information about flow direction and pattern.

A typical evaluation for initial diagnosis of PAD consists of several or all of the following procedures:

Ankle Brachial Index (ABI) Measurements: Estimating the ankle brachial index (ABI) is the simplest and most commonly used test for detection and diagnosis of PAD. In ABI measurements a blood pressure cuff is placed above the ankle and inflated. Peak systolic pressure of the dorsalispedis and posterior tibial arteries is obtained by a Doppler device. ABI is calculated by dividing the ankle pressure by the highest brachial pressure of either arm. In symptomatic patients, abnormal ABI indicates the presence of hemodynamically significant disease. Typically, the index is great than 1.0 in disease-free patients, it decreases to 0.5-0.9 in subjects with claudication and to even lower values in patients with rest pain and tissue loss [3].

ABI may result in inaccurately elevated measurements in diabetic and renal failure patients, who may present with incompressible lower extremity arteries due to calcification. Using toe instead of calf pressure measurements is an alternative way to calculate ABI in this patient cohort [3, 30]. In patients with mild arterial narrowing, the sensitivity of the ABI test can be improved by taking pressure measurements after an exercise challenge such as walking on a treadmill until claudication occurs or for 5 minutes if there is no pain [30].

Segmental Limb Systolic Pressure Measurements: Obtaining pressure measurements from multiple arterial segments is an extension of the ABI tests that can provide information about the primary location of arterial narrowing. In addition to estimating ankle pressure, measurements are obtained from the calves and thighs (Figure 2.1). Pressure difference of more than 20 mmHg between two adjacent segments is indicative of hemodynamically significant occlusive lesion located between the two segments [30].

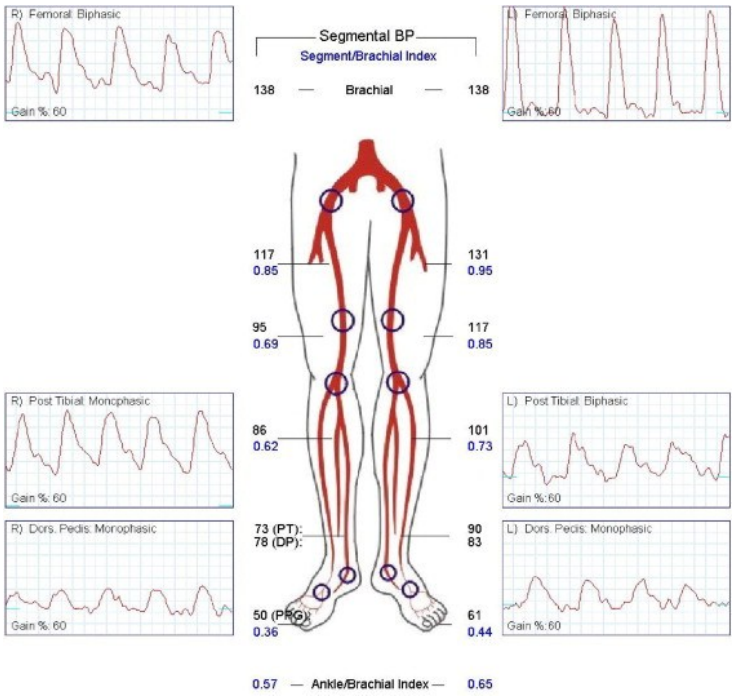

Figure 2.1. Ankle brachial index (ABI) evaluation shows an ABI of 0.57 in the right leg and 0.65 in the left leg and multilevel segmental pressure differentials. Modified from [17].

Occlusive lesion detection accuracy with segmental limb pressure measurements can be improved by combining this procedure with pulse volume recordings.

Pulse Volume Recordings: In this procedure blood pressure cuffs are placed around the limbs at the level of the calves and thighs. A plethysmograph is connected to the cuffs to record pulse volume changes.

Doppler Velocity Waveform Analysis: Healthy vessel segments exhibit unique arterial pressure wave forms that can be obtained by Doppler ultrasound. Changes in the shape and amplitude of the pulse waveform can be indicative of PAD.

(Color) Duplex Ultrasound: An inherent problem of ABI and segmental pressure measurements is the inability to precisely localize an existing stenosis. In this regard, color duplex sonography is a superior tool compared to Doppler alone. Color duplex sonography permits actual visualization of the vessels (Figure 2.2) and provides information about vessel wall changes, degree of stenosis, and post-stenotic flow disturbances.

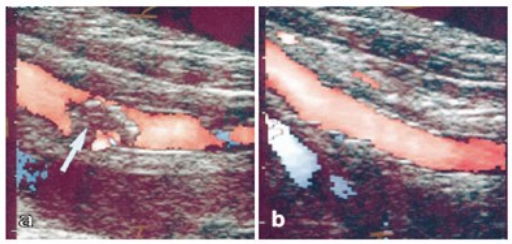

Figure 2.2. Color duplex ultrasound findings before (a) and after (b) stenting of an external iliac artery stenosis. Modified from [18].

Duplex ultrasound is particularly useful for visualization of large, superficial vessels such as the femoral arteries. The tool is used for evaluation of the patency of stented femoral arteries and bypass grafts. However, assessment of the entire vascular tree is imprecise due to the location and small caliber of the distal lower extremity arterial branches. Planning a percutaneous or open surgical intervention with duplex ultrasound as a sole tool is currently inadequate [3]. When the non-invasive vascular tests are inconclusive or are an intervention is contemplated, patients typically undergo additional imaging with either CTA or MRA.

2.2.2. Digital subtraction angiography (DSA)

DSA is the gold-standard for diagnostic imaging of PAD patients [32]. It enables large field-of-view (FOV) imaging with the highest possible in-plane resolution compared to other modalities. However, DSA requires catheterization, nephrotoxic contrast, and exposure to high doses of ionizing radiation. The procedure is associated with major risks such as allergic reactions, infections at the site of vascular access, iatrogenic arteriovenous fistulas, hematomas, and dissections. Complications are reported to occur in 0.17-7% of procedures, depending on the arterial viability, the size of the catheter, the experience of the clinician, and the location of the vascular access. Given the invasiveness of the procedure, its applications is now limited to patients who require a surgical or percutaneous procedure for therapeutic purposes [33, 34].

2.2.3. CT Angiography (CTA)

CTA enables visualization of the entire peripheral vascular tree and offers information about lesion length, diameter, and morphology, as well as degree of calcification, and status of distal runoff vessels. In a CTA exam, the patient is placed in the gantry supine, feet-first. Given the large superior-inferior coverage of the peripheral vasculature, it is not possible to obtain the entire volume of interest in a single scan; instead, a stepping-table approach is used. To selectively visualize the vessels, approximately 100-150 ml of contras material (300 mg iodine/ml) is injected intravenously. Prior to the CTA a test-bolus or bolus triggering scan is performed to appropriately time the angiographic image to the contrast dynamics. Axial slices are reconstructed with slices thickness of 1-1.5mm [31].

A number of studies have compared CTA to the gold-standard DSA, showing comparable diagnostic accuracy and high confidence in clinical decision-making solely based on CTA [35]. In addition, CTA offers evaluation of plaque, calcification, and vascular wall, while DSA depicts only arterial lumen. Technical limitations include the inability to characterize calcified lesions, particularly in smaller vessels, due to beam-hardening artifacts. Primary concerns discouraging the use of CTA are radiation doze and the nephrotoxicity of contrast, which is contraindicated in patients with decreased renal function and renal insufficiency.

Figure 2.3. Contrast-enhanced peripheral MRA.

2.2.4. MR Angiography (MRA)

Prior to the invention of contrast-enhanced MRA (CE-MRA) in the nineties, peripheral MRA was typically performed with a non-contrast technique, known as Time-of-Flight (TOF). Nowadays, TOF has been virtually replaced by CE-MRA primarily due to scan time considerations [36]. CE-MRA is similar in set-up and diagnostic quality to CTA.

CE-MRA methods rely on an injection of contrast material, which alters the magnetic properties of blood. Peripheral MRA is routinely performed with gadolinium (Gd)-based contrast agents (Figure 2.3). Gd is a paramagnetic substance that substantially shortens the T_1 relaxivity of its surrounding environment. Following contrast administration into a vein, 3D images are acquired during the first pass of the substance through the arteries. If the acquisition is properly timed such that only the T_1 properties of arterial blood have been altered, while venous and

background relaxivities remain unaffected, contrast differentiation between arteries and background can be obtained [37].

A fast 3D gradient-echo sequence is used for signal detection. As vascular contrast is relatively independent of flow-dynamics, CE-MRA can be used for large field-of-view (FOV) imaging. This feature is particularly important for peripheral MRA, which demands extensive anatomical coverage. Current state-of-the-art peripheral CE-MRA uses a stepping table bolus chase approach where several sequential 3D gradient echo scans are performed to obtain visualization of all arterial branches from the renal to the pedal arteries. Imaging is performed in three to four steps starting from the abdominopelvic region, then the thighs, and finally the calf and pedal arteries.

Since its introduction in the early 1990s [38], Gd-MRA has seen wide spread clinical acceptance for peripheral arterial evaluation. For assessment of hemodynamically significant disease Gd-MRA has reported sensitivities of 89-99.5% and specificities of 95-99% compared to DSA. The method has also undergone a number of technical advances that have allowed shortened acquisition times and ‘time-resolved’ (4D) imaging of contrast kinetics.

Most recently, research efforts in peripheral CE-MRA have focused on reducing contrast dose, accelerating acquisition times to allow improved dynamic imaging, and the introduction of blood-pool contrast agents. The most commonly used Gd-based agents, e.g. Gd-DTPA, are small molecular weight and are rapidly cleared from the vascular space, requiring very fast imaging to capture the first-pass of the agent through the arteries. A blood-pool agent is a type of contrast material that remains in the vasculature longer (up to 1 hour) and allows for prolonged imaging that can be useful for detection of internal bleeding and MR-guided interventions as well as for improved SNR, CNR, and resolution [37].

Advantages of CE-MRA over CTA are no ionizing radiation and the ability to depict lumen of calcified vessels. Limitations include cost, scan time, and metal artifacts from stents and surgical clips. In recent years, the association between nephrogenic systemic fibrosis (see next section) and gadolinium contrast has limited the applicability of CE-MRA in kidney disease patients.

2.3. PAD and Renal Insufficiency

Renal insufficiency is common in patients with PAD due to frequent co-incidence of PAD with diabetes and hypertension. A retrospective study of 1693 patients with PAD found chronic renal insufficiency in 7.3% [39]. Another large study of 5787 patients with rest pain, ischemic ulceration or gangrene found that 30% had moderate renal insufficiency (GFR 30-50 ml/min/1.73 m^2) and 8% had severe renal insufficiency or kidney failure (GFR < 30ml/min/1.73 m^2) [40]. Consequently, diagnostic tests for PAD must be safe in patients with renal insufficiency.

Among the imaging modalities used in PAD evaluation, ultrasonogrphy has no contraindications for patient with renal insufficiency. However, ultrasonography alone is inadequate for planning of surgical procedures because it does not provide accurate visualization of the entire peripheral vascular tree. Among the remaining modalities, both DSA and CTA, given their exposure to nephrotoxic contrast material and ionizing radiation, are unsafe for kidney disease patients. Until recently, CE-MRA was the only diagnostically accurate alternative considered safe when renal disease is present. Recent association between nephrogenic systemic fibrosis and gadolinium contrast has challenged the safety of CE-MRA as well.

Nephrogenic Systemic Fibrosis (NSF) is a condition that presents with swelling and skin thickening of the extremities, causing (1) muscle weakness, (2) inability to flex/extend joints or (3) walk. An estimated 5% of patients experience rapid progression of symptoms that may be life-threatening. NSF, by itself, is not a cause of death, but may contribute to death by restricting effective ventilation or mobility [41].

The pathogenesis of NSF is unknown; however renal insufficiency is a major risk factor for developing the condition. Recently, the use of Gd-based MRI contrast in patients with renal disease has been correlated with the development of NSF [42-46]. Gadolinium, an element of the lanthanide series, is a chief compound of most MRI contrast agents available for clinical use. It is toxic in its base form, but is bound to organic ligands to enable safe administration. The compound is cleared by the kidneys and is considered safe in patients with normal renal function because the contrast is flushed from the body very rapidly. However, in patients with kidney disease, there is a risk that Gd is not fully cleared and could lead to nephrotoxic effects.

The FDA advises against using Gd-enhanced MRI or MRA in patients with moderate to end-stage kidney disease. The cut off recommended by the FDA is estimated GFR < 60 ml/min/1.73 m^2 [47], while the American College of Radiology (ACR) [48] and the European Agency for the Evaluation of Medicinal Products (EMEA) [49] have advised using a threshold of eGFR< 30 ml/min/1.73 m^2.

In summary, the most accurate imaging modalities that are routinely used for diagnosis and treatment planning of PAD are currently contra-indicated in kidney disease patients. DSA and CTA are unsafe due to exposure to nephrotoxic contrast material and ionizing radiation, while the FDA advises against the use of Gd-MRA due to evidence that gadolinium could trigger NSF. There is a clinical need to develop vascular imaging techniques that are safe in patients

with coexisting PAD and renal insufficiency. The goal of this dissertation is to develop an MRA technique for imaging of the peripheral vessels without the need for contrast injection.

Chapter 3

Non-Contrast Magnetic Resonance Techniques for Peripheral Angiography

Magnetic Resonance Angiography (MRA) denotes a group of MRI techniques used for visualization of the arteries and veins. MRA images aid the detection of abnormal vessel narrowing (stenosis), complete blockage (occlusions), or dilation (aneurysm) as well as presence of blood clots. The technical details of a given MRA sequence depend on the target anatomical area as vessel size, orientation, geometry, and flow dynamics vary greatly across the body. MRA techniques can be divided into two major categories: contrast-enhanced (CE-MRA) and non-enhanced angiography. CE-MRA, which was described in detail in chapter 2, is faster and more technically robust than unenhanced methods and is therefore a preferred clinical option.

However, in recent years there has been a renewed interest in unenhanced techniques, determined by two major factors. First, improvements in MRI hardware and software have reduced acquisition times and made non-contrast imaging clinically practical. Second, the use of CE-MRA in patients with moderate to severe end-stage renal insufficiency is contraindicated due to concerns about NSF in this patient population [36]. This chapter reviews the underlying principles and clinical challenges of standard and experimental non-contrast techniques used for visualization of the peripheral arteries, where *peripheral* denotes all arterial branches from the kidneys to the toes.

Non-contrast MRA techniques rely on flow-induced changes in the longitudinal or transverse magnetization of blood to obtain contrast between the vasculature and stationary background without administration of exogenous contrast material. Four major approaches for artery-background contrast generation exist:

(1) ***Time-of-flight*** techniques rely on differences in exposure to radiofrequency excitation between stationary tissue within the volume of interest and blood protons flowing into the imaging slab from outside the FOV.

(2) ***Phase-contrast MRA*** relays on measurable velocity-induced changes in the phase of the blood signal

(3) ***ECG-triggered subtraction*** techniques relay on the difference in arterial flow velocity between systole and diastole; either gradient echo or fast spin-echo read out can be used

(4) ***Flow-independent*** angiography uses an acquisition that naturally provides bright-blood signal weighting, combined with inversion-recovery and T_2 preparation to null the signal of background tissues.

3.1 Conventional Techniques

3.1.1 Phase-contrast

Phase-contrast angiography is based on the different dynamics that stationary versus moving spins exhibit under the action of bipolar magnetic field gradients. A bipolar gradient is a gradient block which is turned on in one direction for a period of time and then switched to the opposite direction for an equivalent amount of time. A bipolar gradient has no net effect on stationary spins, because the phase accrual during the positive lobe cancels the phase gain accumulated for the duration of the negative lobe. Conversely, spins that have a velocity component along the direction of the gradient will accumulate non-zero phase that is proportional to their velocity.

Playing out a bipolar gradient imparts a phase shift to moving spins, but the effect is not visible on magnitude images. In phase contrast MRA two images are acquired, one with a

positive bipolar gradient (a positive lobe followed by a negative lobe) and one with a negative bipolar gradient (a negative lobe followed by a positive lobe). Upon subtraction, the signal from stationary spins will cancel, while those from moving spins will add, creating an angiogram.

3.1.2 Time-of-Flight (TOF)

Time-of-flight (TOF) has been the most commonly used unenhanced angiographic technique since its introduction in the 1980s. TOF uses gradient-echo readout, in either 2D or 3D. Repeated excitations with short TR and TE lead to saturation of stationary tissues, which exhibit low signal intensity. Inflowing vascular protons in arteries and veins have not experienced the excitation pulses and yield high signal. For selective arterial visualization, saturation bands are used to suppress inflowing venous blood. For maximum inflow effect the imaging slices are positioned perpendicular to the major flow direction. Axial slice orientation is most commonly used as for most applications the flow is in the head-foot direction [36, 37].

Today, the most common clinical application of TOF angiography is the examination of the intracranial vessels. Prior the introduction of CE-MRA, 2D TOF was also the method of choice for peripheral angiography. Overall, 2D TOF imaging of the lower extremities has been replaced by CE-MRA primarily due to prolonged acquisition times and tendency to cause pseudostenosis due to undesirable saturation of in-plane vessel branches [36, 37].

3.2 Novel Approaches

3.2.1 Inversion-Recovery Prepared Inflow MRA

Balanced steady-state free precession (b-SSFP) is a gradient echo sequence that is commonly used in cardiovascular MRI as it provides high signal-to-noise (SNR) ratio and intrinsic T2/T1

contrast weighting, producing bright-blood visualization of the vasculature with minimal dependence on flow [50]. Tissues with high fat or water content have T_2/T_1 weighting similar to that of blood and also appear bright on b-SSFP images. For angiographic applications, b-SSFP is typically combined with inversion-recovery (IR) preparation to suppress background signals and to allow differentiation between arteries and veins.

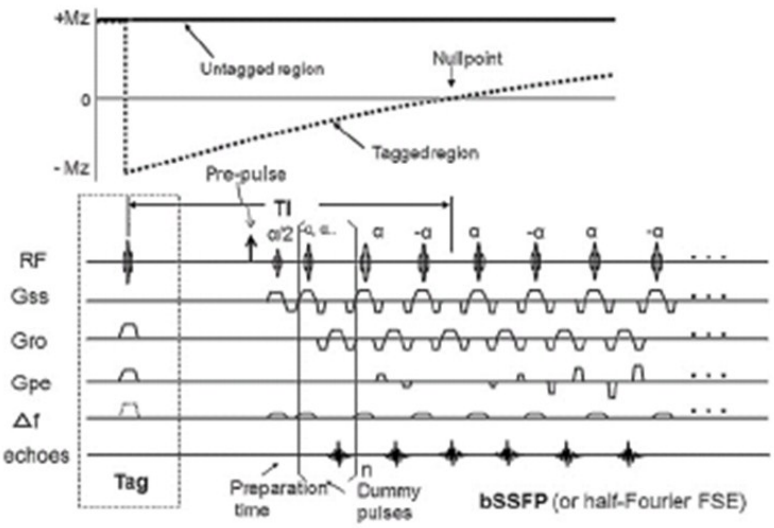

Figure 3.1. Principle of IR b-SSFP MRA. Modified from [43].

Balanced SSFP readout, prepared with a single IR pulse (IR b-SSFP MRA), has been developed for non-contrast evaluation of fast-flowing vascular beds such as pulmonary, carotid, and renal arteries. Similarly to arterial spin labeling methods, in IR b-SSFP MRA a spatially selective IR pulse is applied to saturate the region of interest. The IR pulse inverts the spins in the tagged region, which then undergo exponential recovery via T_1 relaxation, while untagged blood flows into the volume of interest (Figure 3.1.). The inversion time (TI) is selected such that data acquisition occurs when background signal is near a null point and sufficient amount of fresh blood spins have entered the region of interest. For arterial imaging, a second IR or saturation pulse can be placed underneath the field-of-view (FOV) to suppress signal from untagged venous blood [51].

The most clinically popular application of IR b-SSFP is renal artery evaluation. Figure 3.2 illustrates the positioning of the imaging slab relative to the IR slab and the resultant bright-blood renal artery angiogram. In the abdomen, the method is usually performed with navigator-gating or respiratory triggering with bellows to avoid respiratory motion artifacts. Clinical validation of IR b-SSFP MRA in patients with renal artery stenosis has yielded diagnostic accuracies in the 90-95% range [14-17] relative to CE-MRA. Studies report respiratory motion artifacts and insufficient inflow of fresh arterial blood to be the most significant diagnosis-limiting factors.

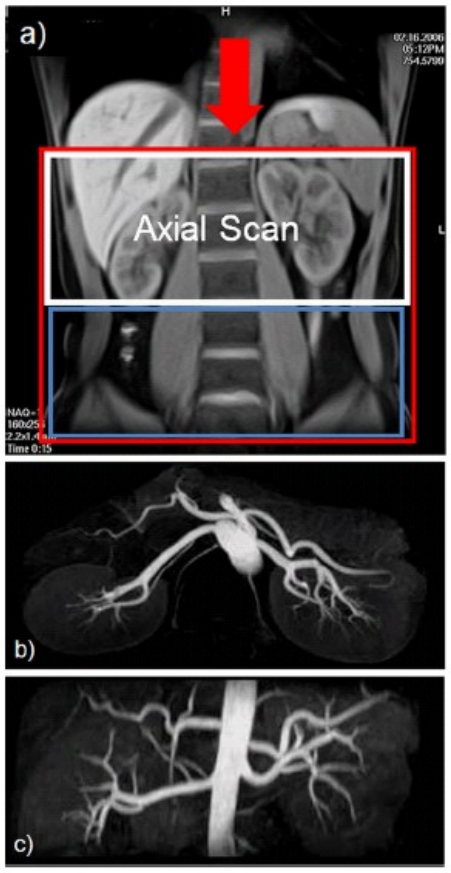

Figure 3.2. (a) Inversion (red) and imaging (white) slab positioning of IR b-SSFP MRA. Resultant renal angiograms in axial (b) and coronal (c) planes. Modified from [43].

3.2.2 Flow-Independent Angiography (FIA):

FIA is the only non-contrast angiographic technique that does not rely on flow-related effects for contrast generation [52]. Similarly to IR b-SSFP, FIA utilizes b-SSFP readout to generate bright-blood signal weighting. The acquisition is prepared with a combination of IR and T_2-Prep preconditioning modules (Figure 3.3) to suppress undesirable background signal, particularly from non-vascular fluids and veins that also appear bright on b-SSFP imaging. Contrast generation exploits differences in T_1, T_2, and chemical shift properties between arterial blood and background species. T_2-weighting (T_2-Prep) is used to suppress muscle and venous signal, while T_1-weighting (IR) is applied to suppress nonvascular fluids relative to arterial blood.

Introduced in 1997 for lower extremity imaging, FIA was the first method to offer 3D volumetric visualization of the calf, including retrograde flow and in-plane vessels, in clinically feasible scan times. However, FIA has not been formally evaluated a patient population and its clinical role remains marginal, likely due to a need for patient-specific sequence parameter optimization prior to scanning.

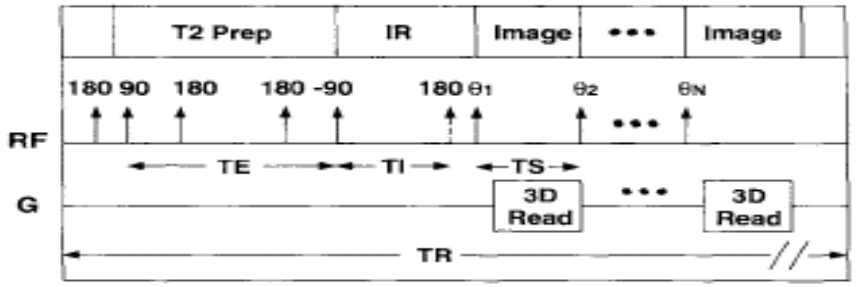

Figure 3.3. Diagram of the T_2-Prep-IR FIA sequence. T_2-Prep-IR combines a T_2-Prep sequence with an inversion recovery period. From [48].

3.2.3 ECG-gated 3D Partial-Fourier FSE Sequence

Among the newer non-enhanced MR angiographic techniques, electrocardiographically (ECG) triggered fast spin echo (FSE) MRA has gained considerable clinical popularity and is currently commercially available by all major vendors. This technique was initially described in 1985 by Wedeen et al. [53] using spin echo imaging and later became clinically feasible after Miyazaki et al. [8] substituted the spin-echo acquisition with a more time-efficient partial-Fourier FSE approach. The method exploits differences between systolic and diastolic arterial flow velocity (Figure 3.4). Arteries demonstrate flow void during systole due to signal loss caused by fast flow. In contrast, during diastole, slow-flowing arterial blood appears bright. Bright-blood MR angiograms are obtained by subtracting systolic from diastolic images. Background tissues and veins exhibit similar signal regardless of the cardiac phase and cancel out on subtraction.

To date ECG-MRA has been evaluated in six small patient cohorts against either CE-MRA or CTA. Study details and outcomes are summarized in Table 3.1. The method demonstrated high negative predictive values (NPV) for imaging of the pedal, calf, thigh, and aorto-iliac arteries, suggesting that ECG-FSE can have a role as an accurate screening tool. However, screening for peripheral vascular conditions is uncommon and most patients referred for an imaging exam are already symptomatic. Therefore, it is desirable to develop non-contrast techniques that can assess disease severity precisely. When technically successful, ECG-FSE provides arterial visualization with encouraging diagnostic accuracy. However, the technique exhibited serious artifacts leading to poor diagnostic quality in a large number of arterial segments (1-47.2%).

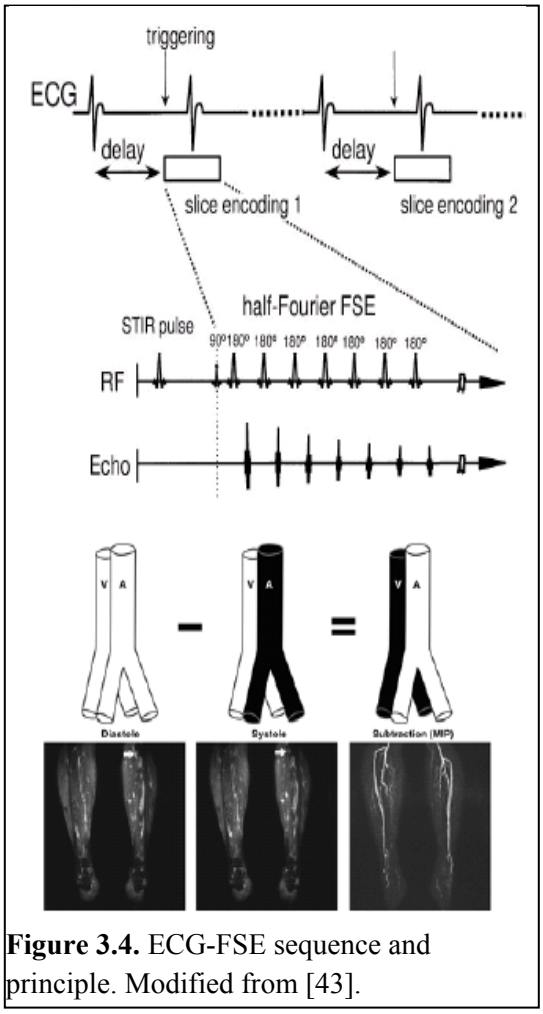

Figure 3.4. ECG-FSE sequence and principle. Modified from [43].

Five out of six studies reported high percentages of non-diagnostic segments in the calf region, identifying two main quality limiting artifacts: (1) patient motion and (2) inaccurate or suboptimal choice of systolic trigger time. Morhs et al [12] found motion artifacts in more than half the patients (19/36, 52.8%). In these cases the assessment of at least one leg was hampered by the artifact. Li et al [54] reported that among all non-diagnostic segments 70% were caused by suboptimal systolic trigger, frequently caused by flow characteristic differences between the two legs.

Three studies [9, 11, 12] evaluated ECG-FSE in the thigh region, reporting higher image quality ratings compared to the calf station, likely due to the fact that the thighs are less susceptible to patient-induced motion artifacts.

ECG-FSE was used for abdominal imaging in only one study [11], which reported non-diagnostic image quality in 10% of all segments and relatively poor positive predictive value (PPV) of 56%. The main diagnosis-limiting factor was undesirable arterial signal loss even in diastole, caused by relatively fast diastolic flow velocities observed in the aorta. This signal loss resulted in insufficient contrast between systolic and diastolic arterial signal and false positive results. Another study [54], which examined only the calf region, stated that imaging of the abdominopelvic area was not attempted due to lack of robust performance of ECG-FSE in this region. When technically successful, ECG-FSE revealed a tendency to overestimate the degree of stenosis. This was typically attributed to T_2-blurring effects caused by relatively long duration of the acquisition window.

The current implementation of ECG-FSE suffers from four main technical limitations. First, the method is unsuitable for abdominopelvic imaging due to high diastolic flow in the aortoiliac arteries and susceptibility to respiratory motion artifacts. Second, in the event of asymmetric disease in the lower extremities, appropriate trigger delays for each leg will differ. Third, the relatively long acquisition window needed to perform single shot acquisitions results in blurring and motion artifacts. Finally, the technique is susceptible to patient-induced motion artifacts as it relies on subtraction of two image sets acquired over the course of 3-5 minutes.

Study	Year	Journal	# of subjects/ area	Field [T]	SS [%]	SP [%]	PPV[c] [%]	NPV[d] [%]	% non-diagnostic segments
Lim	'08	JMRI	36/calf	1.5	92.4	92.1	78.6	97.5	47.2
Haneder	'10	Eur Radiol	36/calf	3.0	100.0	72.7	72.9	100.0	47.0
Mohrs	'11	Eur Radiol	50/calf, thigh, abdomen	1.5	83.5[a] 75.0[b] 93.2[c]	89.9[a] 84.4[b] 82.5[c]	56.3[a] 57.2[b] 65.4[c]	97.2[a] 97.6[b] 98.0[c]	10.0[a] 4.0[b] 8.0[c]
Li	'11	Eur Radiol	64/ calf	3.0	91.9	80.8	87.2	87.5	11.3
Gutzeit	'11	Eur Radiol	42/pedal, calf, thigh	1.5	85.5	95.8	88.6	94.4	1.7[b] 11.6[c] 30.2[d]
Nakamura	'11	MRM	13/calf, thigh, pelvis	1.5	97.0	96.0	88.0	99.0	0.0

Table 3.1. Clinical experience with ECG-FSE
[a] Denotes aorto-iliac a.; [b] Denotes thigh a.; [C] Denotes calf a.; [d] Denotes pedal a.;
SS *Sensitivity*; SP *Specificity*; PPV *Positive Predictive Value*; NPV *Negative Predictive Value*;

3.4 Summary

To our knowledge existing non-contrast MRA techniques either do not have extensive clinical validation or suffer from known limitations when applied for peripheral imaging. The following chapters describe experiments aimed at designing a robust protocol for a three-station peripheral MRA without contrast. We combined ECG-FSE and IR b-SSFP MRA where ECG-FSE was used for imaging of the calf and thigh regions, while IR b-SSFP was used for the abdominopelvic area. To overcome existing limitations (1) the coverage of IR b-SSFP is extended by utilizing four preparation pulses (Chapter 4 and 5) and (2) the technical robustness of ECG-FSE is improved by implementing it with two separate sagittal slabs and interleaved acquisition of systolic and diastolic data (Chapter 6 and 7).

Chapter 4

QIR MRA Sequence for Non-contrast Abdominal MRA

The material presented in the chapter has been published in a peer-reviewed journal under the following title:

Atanasova IP**,** Kim D, Lim RP, Storey P, Kim S, Guo H, Lee VS. *Noncontrast MR angiography for comprehensive assessment of abdominopelvic arteries using quadruple inversion-recovery preconditioning and 3D balanced steady-state free precession imaging*. Journal of Magnetic Resonance Imaging 2011; 33: 1430-39 [55].

4.1 Introduction

Non-invasive assessment of aortoiliac and renal arteries is crucial for diagnosis of renal artery stenosis, and inflow peripheral arterial disease (PAD). Inflow-based NC MRA with 3D balanced steady-state free precession (b-SSFP) readout and a slice-selective (SS) inversion recovery (IR) pulse has been developed for evaluation of renal arteries [13] and validated in patients with renal artery stenosis [14-17] and renal transplants [56]. IR b-SSFP MRA is typically performed axially with 100 - 120 mm craniocaudal coverage, with a single SS-IR pulse applied transversely to completely overlay the imaging slab and to extend inferiorly for venous suppression. The superior-inferior distance from renal arteries to distal external iliac arteries is on the order of 300 mm. Thus, conventional IR b-SSFP MRA is inadequate for comprehensive assessment of abdominal and pelvic arteries. One approach to extend the coverage is to perform coronal imaging [57], allowing for extended visualization of the aorta. However, it is challenging to find

an inversion time that is sufficient to allow unsaturated arterial blood to reach the distal iliac arteries without substantially compromising background suppression. To our knowledge an NC MRA technique that can provide craniocaudal coverage from renal to distal iliac arteries with adequate background suppression in a single acquisition has not been reported.

In this study, the craniocaudal spatial coverage of IR b-SSFP MRA was extended by utilizing four IR pre-conditioning pulses. The objectives of this work were to develop an NC MRA pulse sequence for extended coverage of the abdominopelvic arteries and to evaluate its performance in healthy controls and patients.

4.2. Materials and Methods

Quadruple IR pulse scheme (QIR-MRA) was designed to achieve: i) craniocaudal coverage of the abdominopelvic arteries from suprarenal aorta to distal iliac arteries and ii) adequate background suppression. Figure 4.1 illustrates the pulse sequence. First, a non-selective (NS) IR pulse is applied with inversion time *TI* to invert the longitudinal magnetization (M_z) of all tissues. Immediately after the NS-IR pulse, an oblique sagittal slice-selective (SS) IR pulse overlying the aorta is applied to re-invert aortic spins between the top of the FOV and the aortic bifurcation to equilibrium magnetization (M_0). By "pre-filling" fully-magnetized arterial spins up to the aortic bifurcation, the time needed for fresh arterial spins to arrive at the distal iliac arteries is reduced. Arterial coverage beyond the aortic bifurcation is governed by *TI* and the flow rate of arterial blood.

Subsequent to the NS-IR, M_z of background (e.g., fat, muscle, veins) outside of the sagittal SS-IR excitation slab undergoes magnetization recovery until a short tau IR (STIR) pulse with TI 160 ms is applied to suppress fat and further attenuate background signals. A second SS-

IR pulse, positioned axially and caudal to the FOV, is applied prior to the STIR pulse with inversion time TI_{venous} for suppression of inflowing spins from femoral veins. Imaging is performed with oblique coronal 3D b-SSFP readout with 90° excitation RF pulses and linear k-space ordering to further attenuate background signals. Note that background spins within the sagittal SS-IR excitation slab are fully magnetized prior to the STIR pulse; their signal will be attenuated by the STIR and b-SSFP readout.

4.2.1 Selection of IR Pulse Timing Parameters

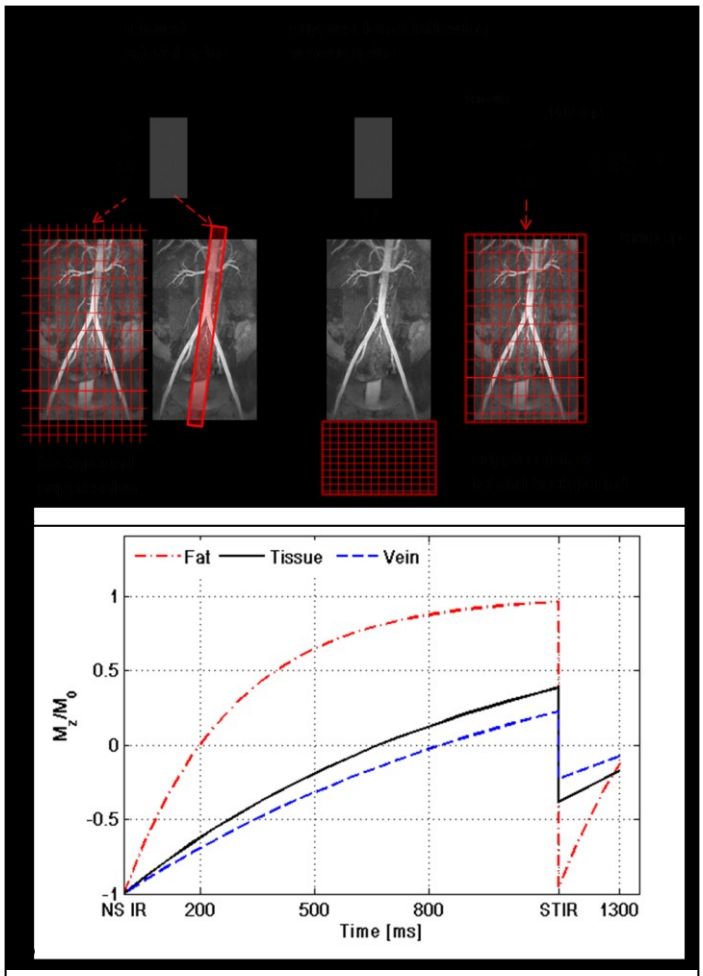

Figure 4.1. QIR-MRA sequence diagram and slab positioning.

Both arterial coverage and magnitude of background M_z are a function of *TI*: longer *TI* extends coverage at the cost of increased background signal and vice versa. We performed *in vivo* velocity measurements to estimate *T I* necessary for sufficient coverage and numerical simulations to calculate *TI* for adequate background suppression. To identify *TI* for sufficient arterial inflow, mean arterial velocity over one cardiac cycle was measured at the origin of the iliac arteries in 14 patients (7 female, 7 male; age range 29-93, mean age 65) undergoing chest or peripheral MRA.

This study was approved by the Institutional Review Board, and informed consent was waived. Measurements were performed with electrocardiogram (ECG) gated phase contrast MRI (2D FLASH, TR 65.3 ms, TE 5.07 ms, FA 20°, TA 18-24 sec, through-plane velocity encoding 100-150 cm/s). Mean arterial velocity, V_{avg}, across all subjects was calculated. To obtain arterial visibility from the renal to the distal iliac arteries, the entire length of the iliac arteries which measure on the order of 200mm has to be filled with unsaturated arterial blood. Assuming constant arterial velocity, *TI* for sufficient coverage was calculated by $TI = 200\text{mm}/V_{avg}$.

In the preliminary study of 14 patients (5 without pathology, 1 with dissecting descending aorta, 3 with infrarenal aneurysm, 3 with enlarged thoracic aorta, 2 with iliac stenosis) presence and severity of disease varied considerably, resulting in a wide range of measured velocities, varying from 4.7 to 23.2 cm/s, with $V_{avg} = 13.8 \pm 4.8$ cm/s. To calculate TI appropriate for volunteers without pathology, two patients whose measurements were obtained within abdominal aortic aneurysms were excluded from analysis, resulting in $V_{avg} = 15.2 \pm 3.1$cm/s and *TI* for optimal coverage of approximately 1300ms. For subsequent *in vivo* QIR-MRA imaging, *TI*was set to 1300ms when no disease was suspected and was prolonged by 400ms when indications for reduced flow rates were present.

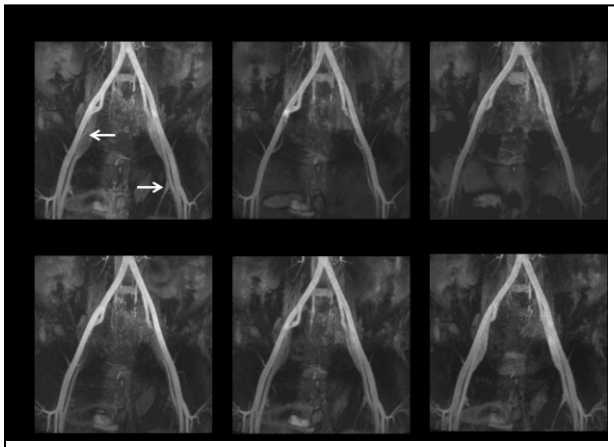

Figure 4.2. Experimental determination of TI_{venous}.

To examine whether the *TI* values identified for sufficient coverage should theoretically provide adequate background suppression, M_z at the center of k-space was calculated using the Bloch equation governing T1 relaxation for three types of background (veins, tissue, and fat). Plots

(Figure 4.1 b) of M_z as a function of time after IR pulses demonstrate near complete suppression of background signals at the center of k-space with *TI*= 1300ms. When *TI* is prolonged to 1700ms (plot not shown), background M_z increases compared to the 1300ms case as follows: venous M_z from $0.07M_0$ to $0.27M_0$, tissue M_z from $0.17M_0$ to $0.35M_0$, and fat M_z from $0.13M_0$ to $0.14M_0$. These values imply that background signal will be brighter with *TI* = 1700ms, but will remain sufficiently low for satisfactory arterial conspicuity. All results were calculated assuming complete inversion of magnetization by IR pulses, ideal slice profile of SS-IR, and tissue T_1 966ms [58], fat T_1 288ms [59], and venous T_1 1200ms [60].

Given the unknown efficacy of the IR pulses outside the FOV, a range of TI_{venous} values were tested in two volunteers (2 male, ages 30 and 49) to empirically determine TI_{venous} for optimal suppression of inflowing venous blood from femoral veins. QIR-MRA was performed with the following settings for TI_{venous} of the caudal SS-IR pulse: none, 300ms, 500ms, 700ms, 900ms and 1100ms. Signal intensity of the iliac veins was assessed to determine TI_{venous} yielding minimal venous signal. TI_{venous} of 500 ms provided best suppression (Figure 4.2). Due to the dependence on transmit RF field (B_1) profile, this observation may vary from scanner to scanner, so that reevaluation of optimal TI_{venous} may be necessary if the sequence is used on a different system.

4.2.2 Human Subject Scanning

Following the determination of our imaging protocol, seven healthy volunteers (1 female, 6 male, age range 23 – 52 yrs; mean age 34 yrs) and 10 patients (4 female, 6 male; age range 57 – 85 yrs; mean age 73 yrs) were studied with the proposed QIR-MRA technique. All patients older than 18 years of age who were scheduled for routine clinical Gd-MRA at our hospital center

were invited to participate in the study. There were no exclusion criteria other than age > 18 years. Among patient who participated in the study, most common clinical indications for imaging included suspected claudication (n=7) or aortic aneurysm (n=3). This study was approved by the Institutional Review Board, and written informed consent was obtained from all subjects. Imaging was performed on a whole-body 1.5T system (Avanto, Siemens Healthcare, Erlangen, Germany; maximum gradient strength = 45 mT/m; slew rate = 200 T/m/s). Radio-frequency excitation was performed using the body coil; two body coil arrays and a spine coil array were employed for signal reception.

***Non-contrast MRA*:** A three-plane dark-blood Half-Fourier acquisition single-shot turbo spin echo (HASTE) scout scan was used for image planning. Subsequently, QIR-MRA was performed using an oblique coronal imaging slab, oriented along the abdominal aorta, with respiratory bellows for triggering (20% end expiration). Imaging parameters included: TR 1 respiratory cycle, TE 1.7ms, FA 90°, BW 1042 Hz/pixel, 60 k-space lines per shot, 2 shots per partition, generalized autocalibrating partially parallel acquisitions (GRAPPA) [61] effective acceleration factor 2.7, FOV 400 mm x 400 mm, 60-80 partitions, nominal slice thickness 1.7 mm, acquisition matrix = 320 x 307, slice resolution 65 %, phase oversampling 10 %, slice oversampling 20-40 %, spatial resolution 1.3 mm x 1.3 mm x 1.7 mm. IR parameters included: NS IR pulse with *TI* between 1300ms and 1700ms as detailed below; 20-60mm thick IR pulse oriented in oblique sagittal plane overlying the abdominal aorta (inversion time 1280ms); 200 mm SS-IR pulse positioned axially immediately inferior to the FOV(TI_{venous} = 500ms); STIR with inversion time 160ms.

All volunteers underwent imaging using the aforementioned protocol. In addition, one of the control subjects (male, age 29) was imaged with the sagittal SS-IR pulse turned off to

illustrate the utility of the re-inversion pulse. The effect of the position and thickness of this pulse was further investigated in a volunteer with known scoliosis (female, age 51). Imaging was performed with *TI* = 1300ms for two positions of the sagittal slab and repeated with *TI* = 1500ms to illustrate the influence of *TI* on arterial visibility and background suppression. Four patients were imaged with *TI* = 1300ms; in six patients *TI* = 1700ms was used in view of indications of reduced flow rates (e.g., age ≥ 70years, known aneurysm).

Gd- MRA: Bolus-chase gadolinium-enhanced MRA was acquired after injection of 30 mL of dilute contrast (22.5mL Gd-DTPA) at 2mL/s (in subjects referred for abdominal MRA) or initially at 2mL/s for 20mL of dilution, then at 1mL/s for 10mL of dilution and a 20-mL saline flush (in subjects referred for three-station peripheral MRA). Timing was based on time-to-peak enhancement of the distal infrarenal aorta and a standard formula [62]. The 3D T1-weighted FLASH sequence was performed with the following parameters: TR/TE 2.9/0.9 ms, FA 25˚, nominal voxel size 1.4 mm x 1.3 mm x 1.4 mm, slice resolution 62%.

4.2.3 Image Quality Assessment

Qualitative Assessment: All data were de-identified and randomized for blinded review by two radiologists with 4 and 5 years MRA experience who independently scored the images. Source images were used for both QIR-MRA and Gd-MRA evaluation. Eight vascular segments per subject (suprarenal artery, right and left renal artery, infrarenal artery, right and left common iliac, right and left external iliac) were assessed for diagnostic quality on a 4-point scale

Figure 4.3. Representative results obtained with QIR-MRA in a healthy volunteer (a) without and (b) with the sagittal re-inversion slab.

(0 = non-diagnostic, 1 = partially evaluable, 2 = mostly evaluable, 3 = fully evaluable). Presence of artifacts was recorded on per segment basis. Each image received an overall diagnostic-quality score based on the same scale.

Quantitative Assessment: Prior to quantitative assessment, 5mm thick axial reconstructions of all 3D data sets were obtained on an independent workstation (Leonardo, Siemens Healthcare). Region-of-interest (ROI) analysis was performed on 12 of the resultant slices, grouped in 4 sets of 3, representative of the following arterial segments: suprarenal, infrarenal, common iliac, and external iliac. Arterial (S_A) and venous (S_V) signal intensities were estimated as the mean intensity of all pixels contained within ROIs drawn to include the entire vessel lumen. Common and external iliac S_A and S_V were calculated by averaging the intensities of the left and the right branches. ROIs for background signal (S_B) estimation were placed over the right lobe of the liver for suprarenal slices and over the iliopsoas muscle for all remaining segments.

Signal-to-noise and contrast-to-noise ratio measurements were not performed due to the spatially inhomogeneous (i.e., g-factor) noise produced by GRAPPA reconstruction. Instead, relative signal contrast ratio between artery and background muscle, CR_{A-B} (= $(S_A-S_B)/S_A$), as well as between artery and vein, CR_{A-V} (= $(S_A-S_V)/S_A$), were estimated for source QIR-MRA images and for source and subtraction Gd-MRA images. To evaluate the efficacy of venous suppression, vein-to-background contrast, CR_{V-B} (= $(S_V-S_B)/S_A$), was also measured. Average CR_{A-B}, CR_{A-V}, andCR_{V-B} were calculated for the above-identified segments and for the entire image.

4.2.4 Craniocaudal Arterial Coverage

Maximal visible length of the common and external iliac arteries obtained with QIR-MRA was measured as a fraction of total "Iliac" length. The latter was defined from aortic bifurcation to origin of profunda femoris. One radiologist reviewed the axial reconstruction images and recorded the last slice position in which the iliac segments were diagnostic. Visible length of the iliacs was measured between this slice position and the aortic bifurcation. Longitudinal views of the iliac segments, obtained by curved multi-planar reconstructions, were used for all measurements to control for differences in vessel geometry and orientation of the imaging slab.

4.2.5 Statistical Analysis

Diagnostic quality scores of QIR-MRA images obtained in patients were compared to the reference standard (Gd-MRA) with a Wilcoxon signed rank test. A paired Student's t-test was performed to determine the statistical significance of differences in $C_{A\text{-}B}$, $C_{A\text{-}V}$, and $C_{V\text{-}B}$ between: a) source QIR-MRA and source Gd-MRA, and b) source QIR-MRA and subtraction Gd-MRA. In all tests, a P value < 0.05 was considered to be significant. Microsoft Office Excel version 12 was used for all analyses.

4.3 Results

Non-contrast angiograms were successfully obtained with quadruple IR b-SSFP in all subjects. QIR MRA scan duration was respiratory-rate dependent and averaged 7.0 ± 2.3 minutes.

4.3.1 Effect of sagittal SS-IR Pulse on Craniocaudal Coverage and Image Contrast

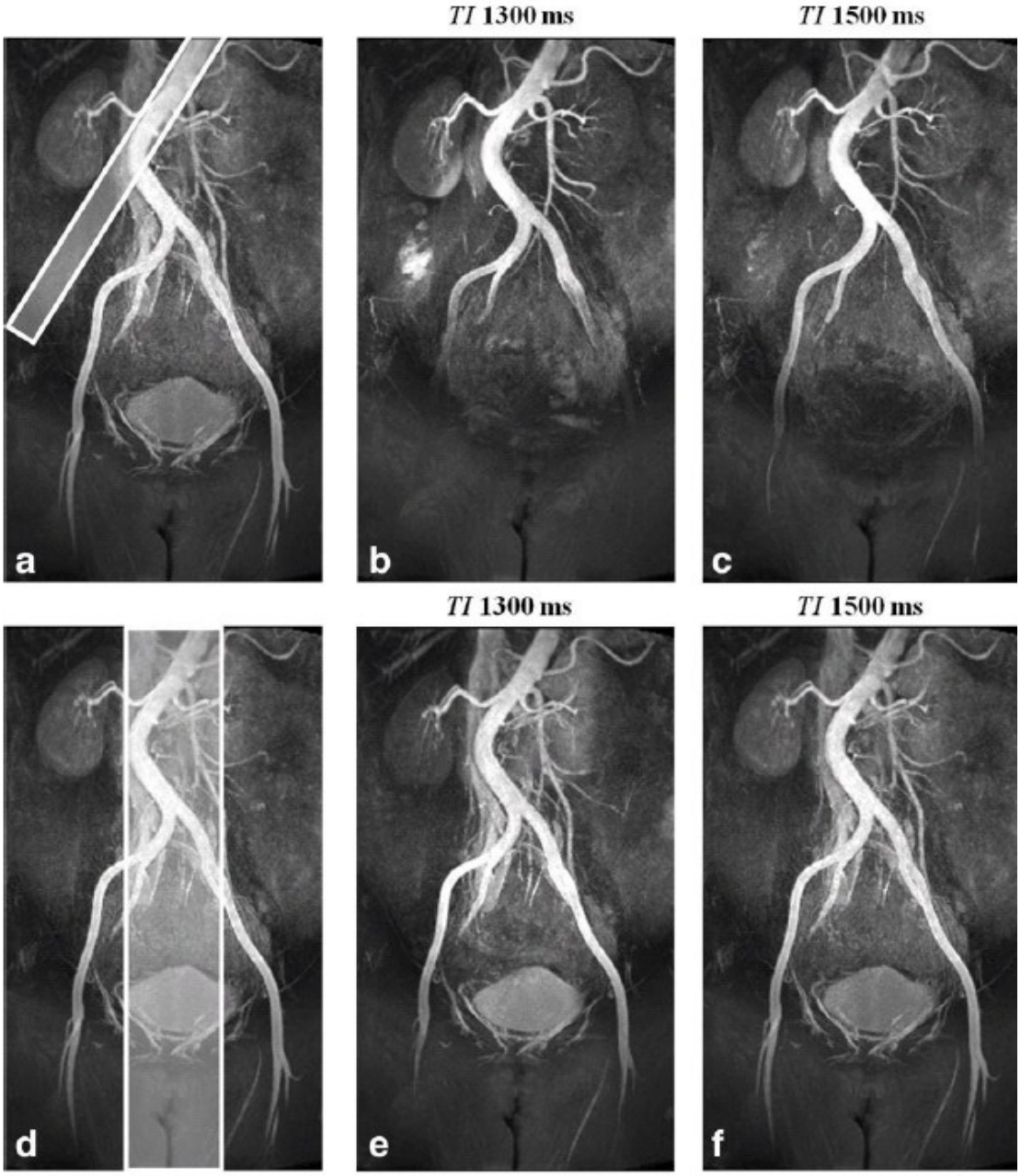

Figure 4.4. Sub-volume MIP of NC MRA (a, b) and full volume MIP of subtraction CE MRA (c)obtained in a 66 year old patient. CR_{A-B} = 0.92 for NC MRA, comparable to subtraction CE MRA (CR_{A-B} = 0.98) and higher than source CE MRA (CR_{A-B} = 0.86).Increased background signal intensity, coincident with the location (a) of the reinversion pulse, was observed with NC MRA in the vena cava (horizontal arrows), lymph nodes (arrow head), bowel, and bladder (vertical arrows). Anterior-posterior coverage of NC MRA was smaller than that of CE MRA causing the truncated appearance of the internal iliac arteries. NC MRA depicted mild infrarenal aortic atherosclerosis and left internal iliac artery origin stenosis in agreement with CE MRA.

Figure 4.3 shows representative NC MRA images acquired with and without the SS-IR pulse, with all other parameters the same. With *TI* set to 1300 ms in both cases, the application of the SS-IR pulse increased craniocaudal coverage by approximately 170 mm without prolonging inflow time at the expense of brighter background coincident with the location of the re-inversion pulse. Figure 4.4 shows results obtained in the volunteer who presented with scoliosis. When the reinversion slab overlaid only half of the infrarenal aorta (Figure 4.4 a), arterial coverage was limited to the common iliac arteries with *TI* of 1300 ms (Fig. 4.4b). Coverage, measured distally to the aortic bifurcation, was extended from 140 mm to 185 mm when *TI* was prolonged to 1500 ms (Fig. 4.4c). It was also possible to extend arterial conspicuity without increasing *TI* by simply re-orienting and enlarging the SS reinverion pulse to overlay the entire infrarenal aorta (Fig. 4.4e). However, with a thicker SS-IR pulse, $CR_{A\text{-}V}$ decreased by approximately 20% due to reinversion of the vena cava. Reduced contrast between left renal artery and kidney cortex was also observed.

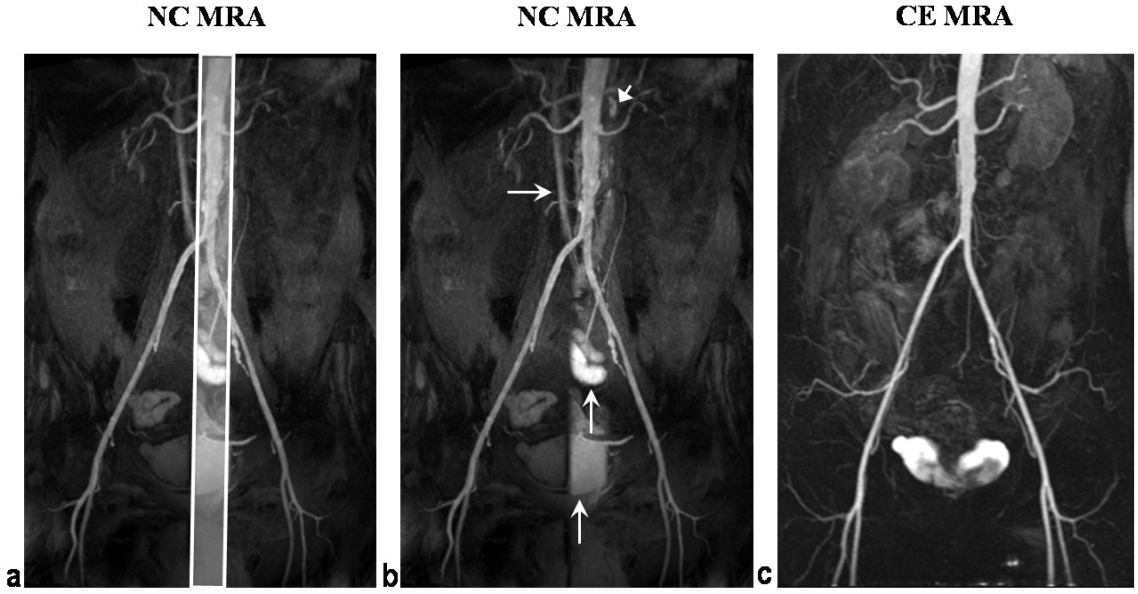

Figure 4.5. Representative QIR-MRA obtained in a 66 y.o. patient. (a) Sagittal IR slab positioning; (b) QIR-MRA; (c) Gd-MRA.

4.3.2 Image Quality

Volunteers: In the seven volunteers overall image quality (Table 4.1) averaged 2.79 ± 0.39 on a scale of 0 to 3, where 3 is maximum. Using individual reader evaluations a total of 112 segments were assessed, of which 86% (96/112) were rated fully evaluable (score = 3). Fifteen (13%) segments received a score of 2 (mostly evaluable), occurring in the external iliac arteries (n=4) and the suprarenal aorta (n=11). The latter exhibited reduced signal intensity likely caused by rapid flow of blood through an off-resonance region. One (1%) segment, part of an external iliac artery, was judged partially evaluable due to insufficient inflow of unsaturated blood. Artery-to-background contrast, $CR_{A\text{-}B}$, obtained in volunteers (Table 4.2) averaged 0.90 ± 0.03 with little variation across segments. Net $CR_{A\text{-}V}$ and $CR_{V\text{-}B}$ were 0.67 ± 0.12 and 0.23 ± 0.10, respectively, signifying adequate venous suppression.

Patients: In the ten patients, 82% (131/160) of all reviewed segments were rated as fully evaluable, while 24 (15%) received a score of 2. Five segments (3%), encountered in the common (n=1) and external (n=4) iliac arteries, were scored as partially evaluable. None were non-diagnostic. Overall image quality score of NC MRA (2.65 ± 0.41) was comparable to that of CE MRA (2.9 ± 0.32) with no statistically significant difference observed between the two (P>0.2). When image quality scores of NC MRA and CE MRA were compared on per segment basis (Table 1), statistically significant differences were found only for the left and right external iliac arteries, with readers describing the following artifacts: insufficient inflow (n=1) and air-filled bowel peristalsis (n = 2).

Overall artery-to-background contrast, $CR_{A\text{-}B,}$ with QIR MRA averaged 0.84 ± 0.06, 14% lower than $CR_{A\text{-}B}$ of subtraction CE MRA. However, $CR_{A\text{-}B}$ of the non-contrast technique was comparable to that of source CE MRA with no statistically significant difference observed

between the two (Table 4.2). CR_{A-V} of QIR MRA averaged 0.55 ± 0.17 and was significantly lower than CR_{A-V} of both source and subtraction CE MRA.

Fig. 4.5b shows a representative QIR MRA image with the maximum image quality score obtained in a 66 year old patient. Overall artery-to-background signal contrast, $CR_{A-B} = 0.92$, was comparable to subtraction ($CR_{A-B} = 0.98$) and source ($CR_{A-B} = 0.86$) CE MRA. Venous signal throughout the image was deemed low by both readers, signifying adequate venous suppression, confirmed by contrast ratio measurements ($CR_{A-V} = 0.78$, $CR_{V-B} = 0.13$). However, medium to high venous signal was observed in a portion of the vena cava due to the sagittal SS-IR pulse. Increased signal intensity, coincident with the location of the sagittal re-inversion pulse, was also encountered in lymph nodes, bladder, and bowel tissue.

4.3.3 Craniocaudal Coverage

Craniocaudal coverage obtained with NC MRA is summarized in Table 4.3. In volunteers, visualized arterial length distal to the bifurcation averaged 209 - 218 mm. Similar inflow distances were observed in patients, corresponding to optimal visualization of 93-96% of the full length of the iliac arteries. In patients, similar coverage was observed for the different *TI* values used (1300 and 1700 ms) likely due to variation of disease severity and cardiac output between the two groups.

The left external iliac artery was successfully completely visualized distal to severe stenosis of the common iliac artery in a 66 year old patient imaged with *TI* = 1300ms (Figure 4.6). In an 80 year old patient (Figure4.7), near complete (96%) depiction of bilateral iliac arteries was obtained distal to an aortic aneurysm by extending *TI* to 1700ms and broadening the SS-IR pulse to completely cover the aneurysm. Suboptimal inflow occurred in one volunteer

(visible left iliac 75%, visible right iliac 77%) and one patient without pathology (visible left iliac 82%, visible right iliac 91%) both imaged with *TI* 1300ms.

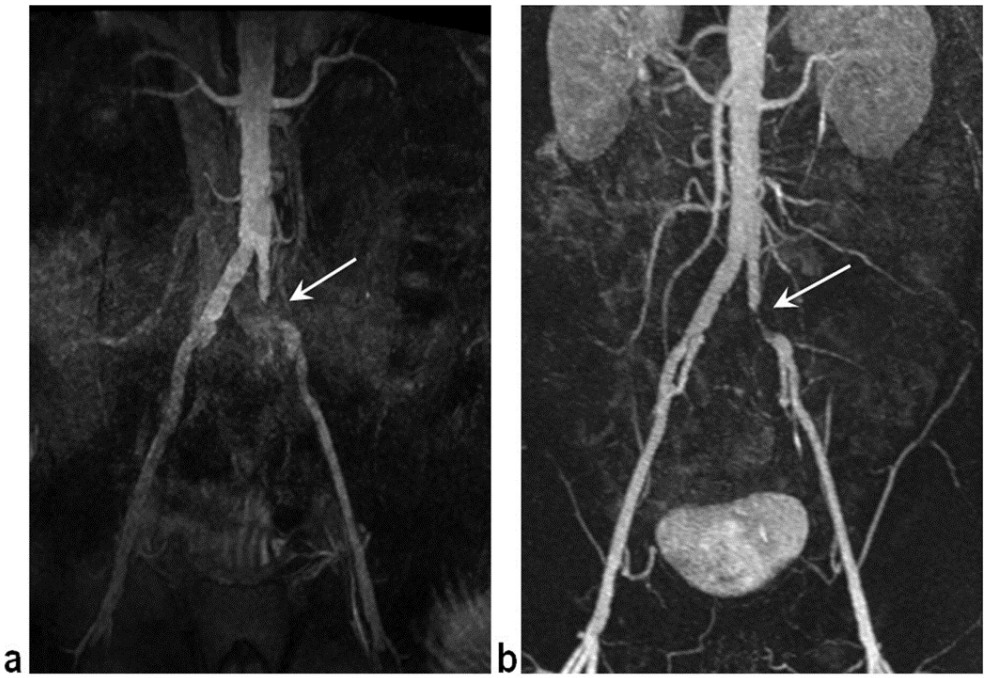

Figure 4.6. In a 66 year old male patient, imaged with *TI* = 1300 ms, NC MRA (a) demonstrated complete visualization of the left iliac segment, distal to sever common iliac stenosis (arrows), confirmed by CE MRA (b). Overall image quality of NC MRA was undermined due to anterior-posterior aliasing. Note that NC MRA resulted in overestimation of stenosis severity.

Vascular pathology was present in five patients. Left and right renal artery stenosis, mild infrarenal atherosclerosis, and infrarenal aortic aneurysm were identified by NC MRA in agreement with CE MRA findings. In one subject, common iliac stenosis was overestimated by NC MRA, compared to the reference CE MRA image (Figure 4.6).

4.4 Discussion

This study describes a new NC MRA pulse sequence for assessment of abdominopelvic arteries, using four IR preconditioning pulses and 3D b-SSFP readout with respiratory trigger. The proposed technique is an extension of the previously described IR b-SSFP MRA sequence for renal angiography. The novelty of the quadruple IR b-SSFP method compared to the renal technique lies in the fact that arterial visualization was extended without prolonging inflow time.

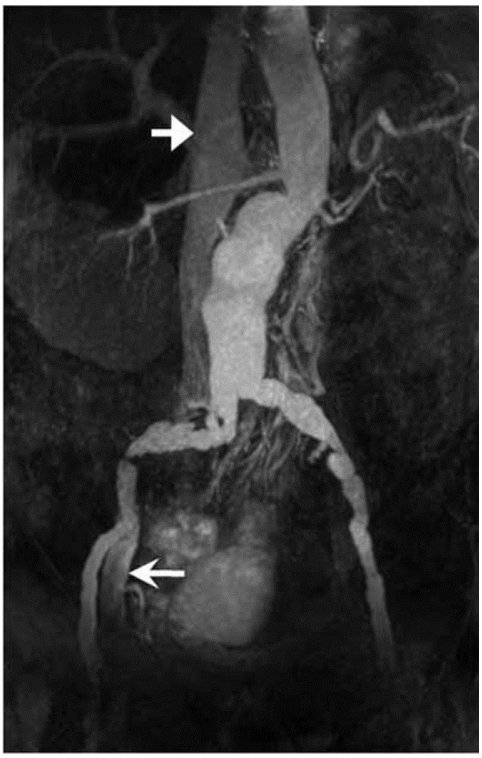

Figure 4.7. 80 y.o. male patient with AAA. The thickness of the SS-IR pulse was extended to completely overlie the aneurysm at the expense of near complete reinversion of the vena cava and partial reinversion of the right external iliac vein (arrows).

Results obtained in controls and patients demonstrate the feasibility to achieve arterial visibility from suprarenal aorta to distal external iliac arteries with sufficient background suppression. As evidenced by CR_{A-B} measurements NC MRA exhibited good static background attenuation in both controls and patients, comparable to CR_{A-B} of source CE MRA. These results reflect the efficacy of the IR preconditioning for background nulling. The STIR pulse was essential for robust suppression of subcutaneous fat and short-T_1 intestinal contents. A STIR pulse was chosen instead of a chemical-shift selective RF pulse, which is more sensitive to static field (B_0) and transmit RF field (B_1) inhomogeneities, especially given a large FOV. The STIR pulse combined with the b-SSFP readout with large excitation angles and linear k-space ordering maintained adequate static tissue suppression even when *TI* was prolonged for extended coverage.

Venous suppression was achieved by two separate mechanisms. Signal from venous spins that remain within the FOV throughout the entire experiment (i.e., venous blood that originally occupies the iliac veins and moves to the vena cava by the start of the readout) is attenuated by the NS-IR and the STIR pulses. Signal from inflowing venous blood, found primarily in the external and common iliac veins, is governed by the inversion time of the caudal SS-IR pulse. Overall venous suppression was adequate with external iliac veins exhibiting more favorable $CR_{A\text{-}V}$ and $CR_{V\text{-}B}$ compared to other segments. This was due to the reinversion effect of the sagittal SS-IR that frequently affected the vena cava and a portion of the common iliac veins.

Respiratory motion in the abdomen and pelvis poses a challenge to the robustness of non-contrast MRA techniques. In prior renal NC MRA studies (9, 10) motion artifacts have been controlled with navigator-gating, which has been reported to provide more robust motion suppression for liver [63] and biliary tree (20) assessment compared to bellows triggering. However, to our knowledge the reliability of navigator gating versus bellows triggering has not been compared in the context of abdominopelvic MRA. Furthermore, in our application the liver-to-diaphragm interface, where the navigator beam is typically positioned, is far from the magnet isocenter. Consequently, it may be difficult to accurately detect the diaphragmatic position for abdominopelvic NC MRA. In this study no significant motion degradation of image quality was observed using bellows triggering. Respiratory-triggered acquisitions, however, may lead to prolonged scan times in subjects with low breathing rates. In these cases it may be helpful to accelerate the pulse sequence using more advanced view ordering schemes [64, 65] or highly-accelerated parallel imaging [61] with a 32-element coil array at the expense of SNR or spatial resolution .

This technique has several challenging aspects that warrant discussion. As craniocaudal coverage beyond the aortic bifurcation is flow-dependent, insufficient conspicuity of the iliac arteries may be anticipated in patients with severely slow flow. In general, coverage may be extended by prolonging *TI* at the expense of increased background signal. Indicators of reduced cardiac output (e.g., hypotension, cardiac failure), monitoring heart rate, or measuring arterial flow velocity using phase contrast MRI prior to NC MRA may guide the selection of an appropriate *TI* and ensure robustness of the technique across a wide spectrum of vascular conditions and blood flow rates.

Secondly, it is important to ensure that the sagittal SS-IR pulse reinverts the entire volume of the abdominal aorta. Failure to do so may reduce arterial visibility distal to the aortic bifurcation. Obtaining scout images of the entire abdominal aorta with coverage up to the heart is therefore necessary for careful planning. The SS-IR pulse also results in a brighter background sagittal "band" that leads to partial visualization of pelvic organs (Figure 4.5). Although this band did not degrade diagnostic quality, minimizing the width of the SS-IR pulse to avoid unnecessary enhancement of background and veins is advocated.

Thirdly, the b-SSFP readout is prone to off-resonance artifacts. Severe signal loss caused by bowel gas occurred in two arterial segments. Reduced signal intensity was frequently observed in the suprarenal aorta, likely due to rapid blood flow through an off-resonance region, given that during initial technical optimization of b-SSFP parameters, this signal loss was observed to deteriorate for longer inter-echo spacing. In this study, complete signal voids were prevented by shortening the excitation pulse duration and increasing the receiver bandwidth to achieve a short TR of 3.3 ms. In a small subset of volunteers the artifact was further reduced with ECG-triggering by acquiring the image during diastole. However, combined use of ECG-

triggering and respiratory gating significantly prolongs the scan time and is impractical for clinical imaging. Previous inflow-based MRA studies (7-10) have utilized ECG-triggering to include at least one systolic period prior to data acquisition. In this study, *TI* was longer than a typical cardiac cycle and, therefore, guaranteed one systolic period prior to data acquisition.

In conclusion, an NC MRA pulse sequence using four IR pulses with 3D b-SSFP readout has been developed for imaging of abdominopelvic arteries. The proposed NC MRA provides high spatial resolution visualization of the aortoiliac and renal arteries with comprehensive craniocaudal coverage and sufficient background suppression in clinically feasible scan times [55, 66]. Preliminary feasibility study in seven volunteers and ten patients showed promising results, so further validation in a larger clinical population was initiated.

Arterial Segment	NC MRA (volunteers)	NC MRA (patients)	CE MRA (patients)
Overall image quality	2.79 ± 0.39	2.65 ± 0.41	2.90 ± 0.32
Suprarenal artery	2.50 ± 0.41	2.50 ± 0.39	2.90 ± 0.32
Left renal artery	3.00 ± 0.00	2.82 ± 0.40	2.90 ± 0.32
Right renal artery	2.93 ± 0.19	2.82 ± 0.40	2.90 ± 0.32
Infrarenal artery	3.00 ± 0.00	3.00 ± 0.00	2.90 ± 0.32
Left com iliac artery	2.93 ± 0.19	2.77 ± 0.47	2.94 ± 0.17
Right com iliac artery	2.93 ± 0.19	3.00 ± 0.00	3.00 ± 0.00
Left ext iliac artery	2.71 ± 0.57	2.59 ± 0.49*	3.00 ± 0.00*
Right ext iliac artery	2.78 ± 0.39	2.50 ± 0.55*	3.00 ± 0.00*

Table 4.1. Image quality ratings for QIR-MRA. * $p < 0.05$.

Arterial Segment		NC MRA volunteers	NC MRA patients	CE MRA (source)	CE MRA (subtraction)
Overall	CR_{A-B}	0.90 ± 0.03	0.84 ± 0.06	0.82 ± 0.04	0.97 ± 0.01
	CR_{A-V}	0.67 ± 0.12	0.55 ± 0.17	0.75 ± 0.10	0.95 ± 0.03
	CR_{V-B}	0.23 ± 0.10	0.29 ± 0.13	0.10 ± 0.06	0.02 ± 0.02
Suprarenal	CR_{A-B}	0.84 ± 0.06	0.78 ± 0.13	0.77 ± 0.09	0.97 ± 0.01
	CR_{A-V}	0.65 ± 0.14	0.51 ± 0.19	0.75 ± 0.17	0.94 ± 0.06
	CR_{V-B}	0.19 ± 0.12	0.27 ± 0.17	0.07 ± 0.07	0.04 ± 0.06
Infrarenal a.	CR_{A-B}	0.90 ± 0.03	0.86 ± 0.06	0.85 ± 0.06	0.96 ± 0.02
	CR_{A-V}	0.60 ± 0.14	0.55 ± 0.16	0.75 ± 0.15	0.95 ± 0.05
	CR_{V-B}	0.30 ± 0.30	0.31 ± 0.12	0.10 ± 0.11	0.03 ± 0.04
Common iliac a.	CR_{A-B}	0.92 ± 0.02	0.86 ± 0.06	0.82 ± 0.08	0.97 ± 0.02
	CR_{A-V}	0.65 ± 0.15	0.56 ± 0.20	0.73 ± 0.15	0.96 ± 0.03
	CR_{V-B}	0.26 ± 0.14	0.30 ± 0.15	0.10 ± 0.08	0.01 ± 0.01
External iliac a.	CR_{A-B}	0.91 ± 0.02	0.84 ± 0.07	0.80 ± 0.08	0.98 ± 0.01
	CR_{A-V}	0.77 ± 0.10	0.58 ± 0.24	0.66 ± 0.17	0.96 ± 0.02
	CR_{V-B}	0.14 ± 0.08	0.26 ± 0.20	0.14 ± 0.11	0.02 ± 0.02

Table 4.2. Contrast ratios for NC MRA in volunteers (n = 7) and NC MRA and CE MRA in patients (n = 10)

Subject Group	Iliac length (right)	Total visible distance (right)	% visible iliac segment (right)	Iliac length (left)	Total visible distance (left)	% visible segment (left)
Volunteers (*TI*:1300ms)	217 ± 8	218 ± 34	94 ± 8 %	205 ± 16	209 ± 48	93 ± 10 %
Patients (*TI*: 1300ms)	212 ± 19	202 ± 25	96 ± 5 %	211 ± 18	207 ± 55	93 ± 9 %
Patients (*TI*: 1700ms)	228 ± 38	217 ± 40	95 ± 4 %	216 ± 31	206 ± 32	95 ± 4 %

Table 4.3. Mean craniocaudal coverage of arterial inflow obtained with NC MRA volunteers (n =7) and patients (n=10)*

*Distance is measured in millimeters distal to the aortic bifurcation

Chapter 5

Clinical Validation of QIR MRA

Following technical optimization of QIR MRA, which was introduced in chapter 4, the non-contrast technique was evaluated in a clinical population to assess its diagnostic accuracy for detection of aortoiliac disease in comparison to conventional CE-MRA.

5.1. Materials and Methods

5.1.1 Patients

All patients scheduled for routine clinical peripheral or abdominal Gd-MRA at our hospital center were invited for participation in this study. There were no exclusion criteria other than age > 18 years. A total of 26 patients (14 female, 12 male) were imaged.. Mean age was 70 years, ranging from 33 to 89 years. Six patients underwent abdominal MRA for evaluation of superior mesenteric artery stent patency (n = 1), suspected abdominal aortic aneurysm (AAA) (n = 3), suspected aortic dissection (n = 1), and vascular screening following endovascular AAA stent and kidney transplant (n=1). Four patients were referred for renal MRA: one for renal artery stenosis (RAS) screening following left kidney nephrectomy and three for suspected RAS. In all other patients (n=14) three-station peripheral MRA was requested for suspected PAD. This HIPAA-compliant study was approved by the Institutional Review Board, and written informed consent was obtained from all subjects.

5.1.2 MR Imaging Protocol

Imaging was performed on a whole-body 1.5T system (Avanto, Siemens Healthcare, Erlangen, Germany; maximum gradient strength = 45 mT/m; slew rate = 200 T/m/s). Radio-frequency excitation was performed using the body coil; two body coil arrays and a spine coil array were employed for signal reception. Patients underwent localization scout scans, followed by QIRMRA of the abdomen, and clinically ordered gadolinium-enhanced MRA protocol. Per clinical request, two subjects were imaged only with QIR MRA due to critically low GFR.

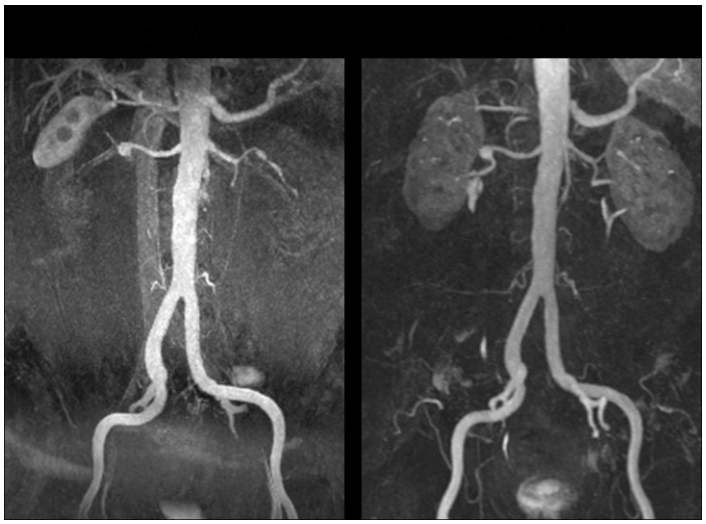

Figure 5.1. Contrast and non-contrast MRA in 82 y.o. male with excellent image quality and no disease.

Unenhanced imaging was performed using an oblique coronal imaging slab, oriented along the abdominal aorta with its superior edge positioned ~2 cm above the origin of the renal arteries. Bellows triggering (20% end inspiration) was used for respiratory motion compensation. Acquisition parameters included: FOV 400 x 400 mm^2, inplane voxel size 1.3 x 1.3 mm^2, 56-66 slices with nominal slice thickness 1.7 mm, slice resolution 65%, TR 1 respiratory cycle, TE 1.7ms, FA 90°, BW 1042 Hz/pixel, 2 shots/partition, GRAPPA factor 2.7, and scan time ~ 5mins. The inversion time that controls inflow of unsaturated arterial blood was heart rate dependent, ranging from 1500-1800 ms, selected to ensure arterial inflow over 2 systolic periods prior to data acquisition.

Breath-held Gd-MRA of the abdomen was performed in an oblique coronal plane, oriented along the abdominal aorta, with 3D T1-weighted Fast Low-Angle Shot (FLASH)

sequence, using in-plane matrix size 336 x 448 mm^2, slice thickness 1.4 mm, slice resolution 70%, flip angle 20˚, BW 1010 Hz/pixel, phase and slice partial Fourier 6/8, parallel imaging acceleration (GRAPPA) factor 2.6. Scan time was 20-23 sec.

Single station Gd-MRA was performed in patients referred for renal or abdominal MRA with FOV = 400 x 400 mm^2, nominal voxel size 1.2 x 0.9 x 1.4 mm^3, TR/TE 3.61/1.2 ms. The imaging slab was centered at the level of the renal arteries. 0.1 mmol/kg gadopentetate dimeglumine (Magnevist: Berlex Laboratories, Wayne, NJ) was injected at 2 mL/sec via automated injector (Spectris, Medrad, Indianola, PA), followed by a 20-mL saline flush, injected at the same rate. Timing was based on a time-to-peak enhancement of the pararenal aorta, measured using a 1-mL test dose and a standard formula [62].

Patients referred for peripheral MRA underwent dynamic imaging of the calves, followed by three-station bolus-chase MRA. A dose of 0.15 mmol/kg Magnevist was injected, of which 0.04 mmol/kg was used for time-resolved imaging and 0.11 mmol/kg for bolus-chase. The bolus-chase dose consisted of 30 mL of dilute contrast, injected initially at 2 mL/s for 20 mL of dilution, then at 1 mL/s for the remained (10 mL) of the dilution and a 20-mL saline flush. For timing, a 1-mL test bolus was used to determine time-to-peak enhancement of the distal infrarenal aorta. The abdominopelvic station of the bolus-chase

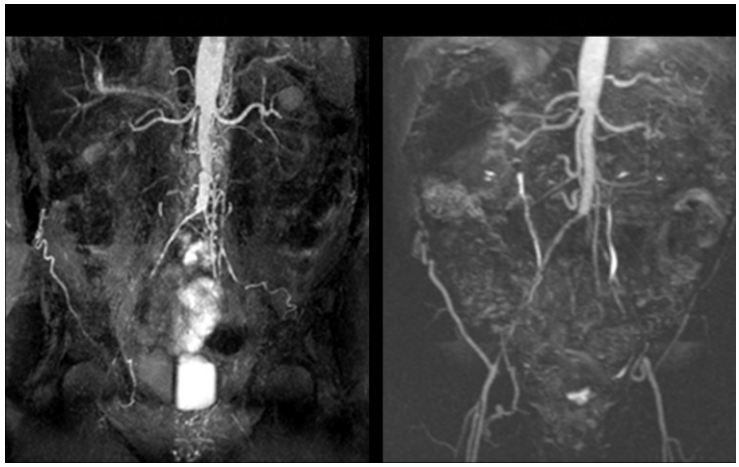

Figure 5.2. Contrast and non-contrast MRA in a 63 y.o. female patient with severe disease.

exam was performed first with the following parameters: FOV = 380 x 500 mm^2, nominal voxel size 1.5 x 1.1 x 1.4 mm^3, TR/TE 3.43/1.09 ms. The abdominal and the thigh stations were placed relative to the calves station, which was positioned to include all anatomy from metatarsal bases to tibial plateau. Thus, the exact location of the abdominal station varied depending on the height of the patient.

5.1.3 Image Evaluation

Two radiologists independently evaluated all images in random order, blinded to patient identity and sequence type. Source and maximum intensity projection (MIP) images of QIR MRA together with pre- and post-contrast source, subtracted, and MIP images of Gd-MRA were loaded on a workstation (Syngo, Siemens, Germany) and made available for review. For Gd-MRA, readers relied on the post-contrast source images for interpretation; source data were used for QIR MRA.

The abdominal arteries were divided into 10 segments per patient: suprarenal aorta, infrarenal aorta, right/left renal artery, right/left common iliac artery, right/left external iliac artery, right/left internal iliac artery origin. Each segment was assessed for disease severity using the following grading system: 0 = no stenosis, 1 = 1-49% stenosis, 2 = 50-99% stenosis, 3 = 100% occlusion. If discrepancies in the disease grading of Gd-MRA segments were found following independent review, a consensus reading was obtained and adopted as a true measure of stenosis. Presence of accessory renal arteries was reported. Abdominal aortic aneurysms, when present, were noted and their maximum diameter was measured. Image quality was rated on a per-segment basis on scale from 0 to 3: 0 = unevaluable, 1 = poor, 2 = fair, 3 = excellent. Respiratory motion, bowel motion, and susceptibility artifacts (0 = present, severely limits

evaluation, 1 = present, but does not limit evaluation, 2 = absent) were also recorded on a per-segment basis.

5.1.4 Statistical Analysis

The accuracy of QIR MRA for detection of hemodynamically significant stenosis was measured in terms of sensitivity, specificity, positive predictive value (PPV), and negative predictive value (NPV) relative to the reference standard, Gd-MRA. Stenosis grading of 2 or 3 (> 50%) was considered significant. Segments not included in the imaging FOV on either sequence were excluded from analysis. Segments that were evaluable on the reference standard, but could not be evaluated on QIR MRA due to poor image quality were counted as an incorrect assessment. Kappa statistics was used to assess interobserver agreement for both QIR MRA and Gd-MRA. Image quality and artifact scores of Gd-MRA and QIR MRA were compared with the Wilcoxon signed rank test. All reported P-values were considered significant when less than 0.05. Analysis was performed in Matlab (The MathWorks, Inc., Natick, MA).

5.2 Results

Excluding results in two patients who did not undergo CE MRA, 452 of 480 potential arterial segments (24 patients, 2 readers per segment) were available for quantitative analysis. A total of 26 potential segments, comprising the right and left internal and external iliac arteries of three patients and the left external iliac of a forth patient, were not included in the FOV on CE MRA. A left renal artery was absent in one patient due to nephrectomy.

Image quality of CE MRA (2.8±0.3) was superior to that of QIR MRA (2.2±0.5); however, 98% of all evaluated non-contrast segments were judged diagnostic. 85% of QIR MRA

segments were rated with fair (50%) or excellent (35%) image quality (Figure 5.1), while 60/452 (11%) segments exhibited poor image quality. Nine (2%) segments were considered non-diagnostic, occurring in the left common and the left internal iliac arteries of one patient due to aliasing; in the suprarenal aorta (n=5) due to banding artifact; and in the external iliac arteries (n=2) due to insufficient inflow of unsaturated blood. Seven (1.5%) segments were non-diagnostic on CE MRA due to mistiming of contrast agent administration.

At the reference standard of assessable CE MRA segments with diagnostic quality, hemodynamically significant stenosis (defined as ≥ 50%) was found in 44/452 (10%) segments (Figure 5.2) These were primarily observed distal to the aortic bifurcation, with only two renal arteries affected by significant disease. Atherosclerotic plaque was detected in the abdominal aorta, but stenosis ≥ 50% was not present. Of all evaluable segments with CE MRA available, overall sensitivity and specificity of QIR MRA were respectively 86% and 95% (reader 1) and 86% and 93% (reader 2). NPV and PPV were 98% and 63% for reader 1, and 98% and 56% for reader 2. The two readers had three false negative readings each (Figure 5.4), and 12 and 15 false positive readings (Figure 5.3). The results of segmental analysis are summarized in Tables 5.1 and 5.2.

The kappa coefficient showed good agreement (0.83) between readers for identification of significant stenosis using QIR MRA.

5.3 Discussion

Our results demonstrate good agreement between Gd-MRA and QIR MRA for detection of disease in the abdomen and pelvis. Overall image quality of QIR MRA was fair (2.2 where 3.0 is highest) with a small percentage (2%) of non-diagnostic segments caused primarily by operator

errors. A relatively high number of segments (10%) had poor image quality on QIR MRA, but diagnostic accuracy was principally not affected in these branches. Segments with poor image quality rating were predominantly located at the edges of the FOV (superarenal and internal iliac artery origin) and were affected by b-SSFP banding and off-resonance artifacts.

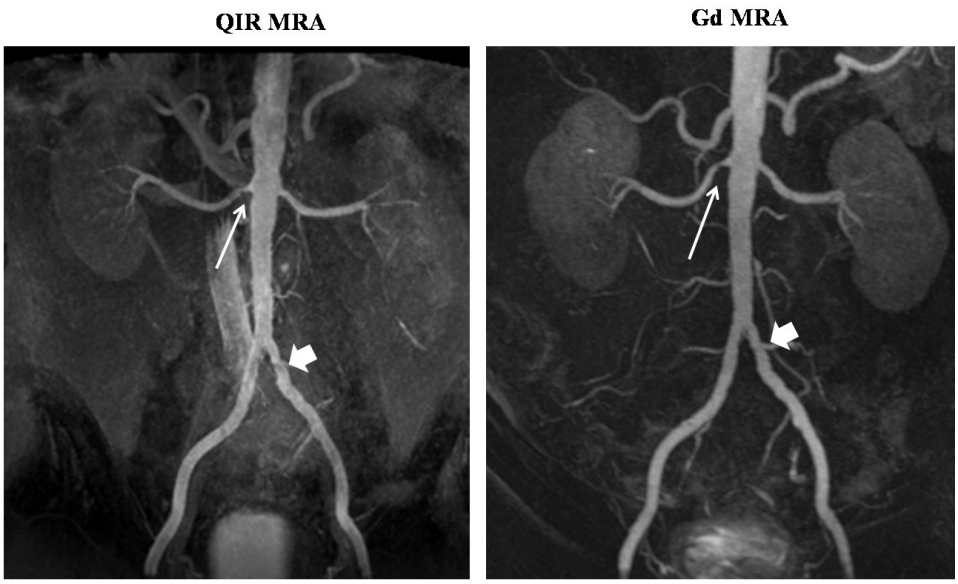

Figure 5.3. QIR and Gd MRA in 80 y.o. male patient with mild disease. QIR overestimated degree of stenosis of the left common iliac artery (arrow head) and the right main renal artery (arrow).

We observed a tendency of the non-contrast technique to overestimate degree of stenosis. As most of the discrepancies between QIR MRA and the reference standard occurred in segments with fair or excellent image quality on QIR MRA, the source of error was likely related to spatial resolution or signal dispersion distal to stenosis. More detailed analysis revealed false positive readings in 19 unique segments, of which six were related to image artifacts. Disease could not be evaluated in four QIR MRA segments deemed non-diagnostic due to anterior-posterior wrap (1 left common, 1 left internal, and 1 right external iliac a. in the same patient) and insufficient inflow of unsaturated blood (right external iliac a.). Poor image quality was likely the cause of disease overestimation in two additional segments: focal pseudo-stenosis

occurred in the right external iliac arteries of two patients due to off-resonance caused by bowel peristalsis. One internal iliac artery had inaccurate readings likely caused by small vessel caliber together with inability to confidently evaluate the segment near the posterior edge of the FOV. In six segments (two renal a., two common iliac a., one external iliac a., and one internal iliac a.) with mild disease on CE MRA, disease overestimation possibly resulted from weak forward flow distal to stenosis.

The remaining six false positive segments had excellent image quality on QIR MRA. On CE MRA images readers found stenotic narrowing in all six segments, but disagreed about disease severity, with consensus reading of mild disease (Figure 5.3). There is clinical evidence that CE MRA may result in inaccurate stenosis grading, typically overestimation, and given the lack of true reference standard in this study, the cause of the inconsistent readings of these six segments is uncertain.

False negative readings occurred in three segments: left internal iliac a. (n = 1), left renal a. (n=1), and right renal a. (n=1). In all of these cases both readers indicated presence of disease on CE MRA images, but disagreed about its severity, with consensus reading of significant stenosis. The inconsistency in the readings of the internal iliac segment likely resulted from poor image quality of QIR MRA caused by artifacts at the posterior edge of the FOV where the segment was located. In the renal artery cases, image quality of QIR MRA was rated fair or excellent and both readers graded the segments as mildly stenotic (< 50%). The discrepancy between QIR-MRA and the reference standard was likely caused by small vessel caliber since accurate quantification of stenosis in small branches is challenging even with CE MRA.

Dependence on flow is a potential limitation of QIR MRA. Based on volunteer studies, we have observed that allowing two systolic events to occur in the interval between the first

inversion pulse and the readout guarantees sufficient inflow of unsaturated blood in the majority of subjects. When feasible, in this study *TI* was set to twice the duration of the patient's cardiac cycle to ensure inflow over two systolic events. However, due to background signal considerations *TI* was restricted to a maximum of 1800 ms in subjects with slow heart rates whose cycle exceeded 900 ms. Reduced signal intensity of the distal external iliac arteries was commonly observed in this patient cohort, but it did not affect overall diagnostic quality with only one external iliac segment deemed non-diagnostic due to insufficient inflow. While

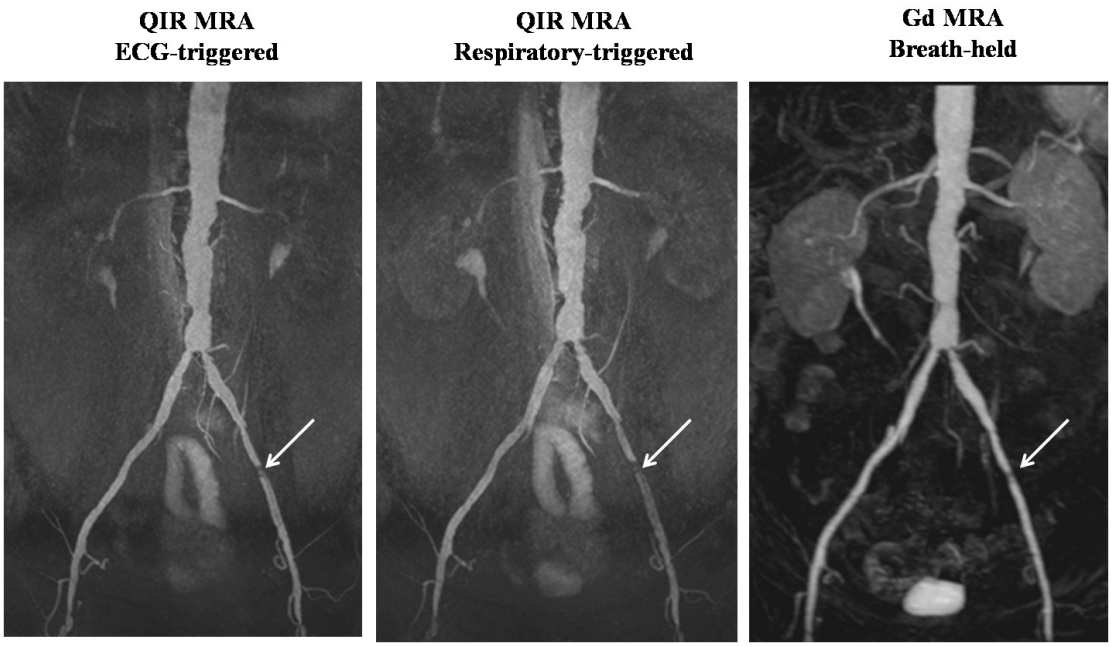

Figure 5.4. QIR MRA and CE MRA in a 75 y.o. female with mild iliac disease. QIR MRA with respiratory triggering resulted in overestimation of left external iliac stenosis (arrow). Using ECG-triggering offered more accurate depiction of the stenotic lesion.

inadequate inflow may be anticipated in patients with severely slow flow, our results indicated that QIR MRA produces consistent superior-inferior coverage across patients.

Dependence on inflow can be problematic in the presence of stenosis. Signal intensity drop distal to mild stenosis was observed in six to eight segments in this study and resulted in disease overestimation. This was likely caused by either reduced forward flow or signal

dephasing caused by turbulent flow. In this study, QIR MRA was respiratory-triggered. This implies that the timing of peak systole (maximum inflow) relative to the acquisition differed from one excitation to excitation, leading to variations in the amount of arterial inflow between subsequent readouts. Furthermore, irregularities in the breathing pattern, particularly ones that shorten the respiratory cycle, could cause reduced or no inflow during some excitations. These inconsistencies possibly exacerbate insufficient coverage and stenosis overestimation. One foreseeable approach to alleviate the problem is to combine respiratory compensation with ECG-triggering, as has been done in prior studies focused on the renal arteries. The use of ECG-triggering eliminated stenosis overestimation in one of our case compared to respiratory-triggering only (Figure 5.4).

This study has recognized limitations, including small number of patients and small number of segments with significant disease. Furthermore, at our institution, MRA findings often dictate management, with angiography performed only if intervention is being considered. As a result, angiographic correlation was not available in any of the patients and gadolinium-enhanced MRA was used as a gold standard, even though the accuracy of CE MRA has been questioned by at least one multicenter trial.

In conclusion, our initial clinical evaluation of QIR MRA shows high negative predictive value for evolution of abdominopelvic arteries. QIR MRA is safe and easily-repeatable and this study suggests that it is also a reasonable alternative when contrast is contra-indicated due to impaired kidney function or when patients are unable to suspend respiration. QIR MRA exhibited a tendency to overestimate stenosis and further validation is necessary to ascertain whether this is a fundamental limitation of the technique or is unique to the protocol of this study [67].

Reader 1

	Accuracy	Sensitivity	Specificity	NPV	PPV
Suprarenal a.	100	N/A	100	100	N/A
Infrarenal a.	100	N/A	100	100	N/A
Renal a.	91	N/A	96	96	N/A
Common iliac a.	98	100	95	100	75
External iliac a.	90	100	90	100	43
Internal iliac a.	88	91	87	96	71
Overall	94	86	95	98	63

Reader 2

	Accuracy	Sensitivity	Specificity	NPV	PPV
Suprarenal a.	100	N/A	100	100	N/A
Infrarenal a.	100	N/A	100	100	N/A
Renal a.	94	N/A	98	96	N/A
Common iliac a.	94	100	88	100	55
External iliac a.	88	100	87	100	38
Internal iliac a.	88	91	87	96	71
Overall	92	86	93	98	56

Table 5.1. Diagnostic Accuracy of QIR MRA.

Reader 1				
	TruePos	**TrueNeg**	**FalsePos**	**FalseNeg**
Suprarenal a.	0	24	0	0
Infrarenal a.	0	24	0	0
Renal a.	0	43	2	2
Common iliac a.	6	40	2	0
External iliac a.	3	34	4	0
Internal iliac a.	10	28	3	1
Overall	19	193	11	3
Reader 2				
	TrueNeg	**TruePos**	**FalsePos**	**FalseNeg**
Suprarenal a.	0	24	0	0
Infrarenal a.	0	24	0	0
Renal a.	0	44	1	2
Common iliac a.	6	37	5	0
External iliac a.	3	33	5	0
Internal iliac a.	10	27	4	1
Overall	19	189	15	3

Table 5.2. Diagnostic Performance of QIR MRA relative to Gd-MRA

Chapter 6

Flow Sensitivity of Fast Spin-Echo Sequences in the Context of Noncontrast Peripheral MRA

Results reported in this chapter have been published in a peer reviewed journal and presented at an international conference under the following titles:

Storey P, Atanasova IP**,** Lim RP, Xu J, Kim D, Chen Q, Lee VS. *Tailoring the flow sensitivity of fast spin-echo sequences for noncontrast peripheral MR angiography*. Magnetic Resonance in Medicine 2010; 64(4):1098-108.

Atanasova IP, Storey P, Lim R, Laine A, Lee VS. *"Effect of flip angle evolution on flow sensitivities in ECG-gated fast spin echo MRA methods at 3T."* Proc. Intl. Soc. Mag. Reson. Med 2009: 3903

Fresh blood imaging (FBI), which involves the subtraction of two 3D fast spin-echo image sets, is a non-contrast technique for peripheral MRA. Technical details of the method as well as its reported *in vivo* performance are discussed in detail in chapter 3. The experiments described hereafter are intended to investigate how the parameters of the fast spin-echo sequence affect its flow sensitivity, and how that in turn impacts the depiction of large and small arteries.

Fast spin-echo sequences with both constant (CFL) and variable flip angle (VFL) pulse trains are commercially available. ‘Constant’ in this case means that the flip angle of the refocusing pulses remains constant throughout the echo train except for the first few pulses, where it is adjusted appropriately to achieve a smooth transition to a pseudo-steady state. In a variable flip angle train, the flip angle is reduced rapidly to achieve a target signal level, and then increased gradually to maintain that signal for much of the remainder of the echo train [68].

Figure 6.1. From left to right: MIP images of the calf, cropped diastolic image, systolic, and MIP image of the popliteal artery. a) VFL with dark artery in diastole b) VFL with bright artery in diastole c) CFL with incomplete flow void.

Originally, FBI employed constant flip angles, but was later implemented with VFL to minimize SAR and to enable the use of very long echo trains without blurring.

Subsequent to the transition to VFL readout, we observed a frequently-occurring artifact in healthy volunteers: severe signal loss at the center of the popliteal artery on MIP images (Figure 6.1a MIP). Upon closer inspection of the source data, unexpectedly low arterial signal was found on the diastolic images (Figure 6.1a diastole). A brief study in a small cohort of patients was conducted to investigate the source of the artifact.

6.1 Preliminary Experiments

6.1.1. Methods

Phantom Experiment: CardioFlow 5000 MR pump (Shelley Medical Technologies, Canada) was used to drive a blood-mimicking fluid (4% glycerol, 96% distilled water, doped with 0.1ml Gd/L for T_1 = 1600 ms, T_2 = 230 ms) through a braid-reinforced Tygon tube with inner diameter of 1.6 cm at 10 constant flow rates ranging from 0 to 60 ml/s. The phantom was imaged with a body phased array coil with the same system and sequence parameters used for the human studies. CFL was performed with 180° and 120° flip angles. Flow velocities corresponding to the pump flow settings were estimated by phase contrast quantification and correlated to the resultant signal intensities of the imaged fluid.

Human Experiments: The distal and proximal lower extremities of 6 healthy volunteers were scanned at 3T (Siemens Tim-Trio) with the VFL (Siemens SPACE, Sampling Perfection with Application optimized Contrasts by using different flip angle Evolutions) sequence; 3 of these subjects were also imaged with the CFL-approach with the following parameters: matrix 320 x 240, GRAPPA factor 3, reference lines 24, BW 977Hz/px, phase half-Fourier, TR = 2 RR intervals, FOV 400 x 272 mm^2 with 2mm-thick slices and 90-104 partitions for the thigh, and 1.5 mm slices with 80-88 partitions for the calf, with centric reordering and using a multichannel peripheral phased array coil. For VFL, additional parameters were TE 18 ms, echo spacing 2.44 ms, turbo factor 72, echo-train duration 88 ms. For CFL, images were acquired with a 120° flip angle with TE 2.7 ms, echo spacing 2.84 ms, turbo factor 72, echo-train duration 102 ms. All acquisitions were single-shot and ECG triggered with trigger delay (TD) of 0 ms for diastole and 200-300ms for systole, determined based on velocity versus time curves obtained by phase contrast flow quantification (2D FLASH, TR 70.3 ms, TE 3.79 ms, FA 20°, venc 100 cm/s). The

arterial CFL and VFL signal intensities (normalized to adjacent muscle) and corresponding velocities (based on phase contrast) were compared for 6 different anatomical regions spanning the entire leg from the femoral heads to the ankle.

6.1.2. Results

In healthy subjects, arterial velocity patterns ranged considerably (Figure 6.2) resulting in MRA images of variable quality (Figure 6.1). Peak systolic velocities were consistently > 15cm/s and varied from 15 to 90 cm/s. Diastolic velocities ranged from 1-8 cm/s, with higher velocities observed in the common femoral (CFA) and distal popliteal (disPop) arteries. Phantom data (Figure 6.3), supported by similar in vivo results (Figure 6.4), demonstrate that flow sensitivities for CFL and VFL vary significantly and explain MRA appearances in subjects (Figure 6.1). At all velocities CFL shows relatively high signal, compared with VFL. Velocity sensitivities depend on the flip angle, with smaller sensitivity range (i.e. velocities over which SI falls rapidly) for lower flip angles (12-30ml/s for 180° and 8-18cm/s for 120°). VFL, which uses even lower FA magnitudes (40°-140°), exhibits a much smaller range of sensitivity with the highest SI below a threshold velocity of 5 cm/s, above which, near complete signal void occurs. With the VFL approach, vessels such as CFA and disPop, where diastolic velocity exceeded 5 cm/s, appear hollow on subtraction MRA (Figure 6.1a MIP) due to the diastolic signal void centrally in the artery (Fig. 6.1a diastole). With CFL the arterial SI is relatively high

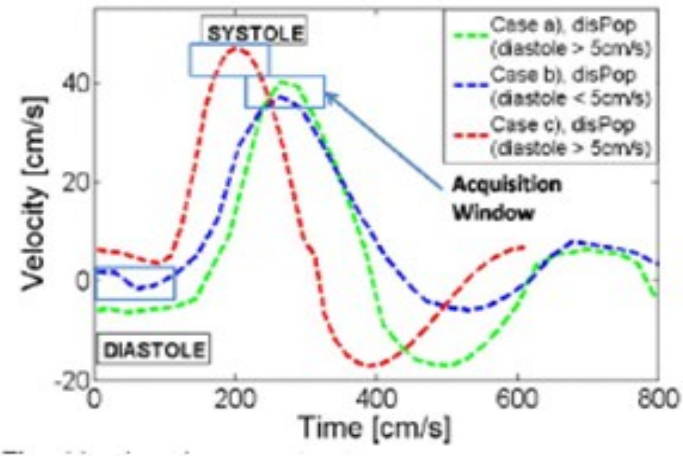

Figure 6.2. *In vivo* phase contrast curves corresponding to images in Figure 6.1.

even at high velocities (Figure 6.1c systole). This could potentially impair image quality due to minimal SI differentiation between systole and diastole, but implementation with flow spoiling gradients, as is typically performed [8], improves the image contrast.

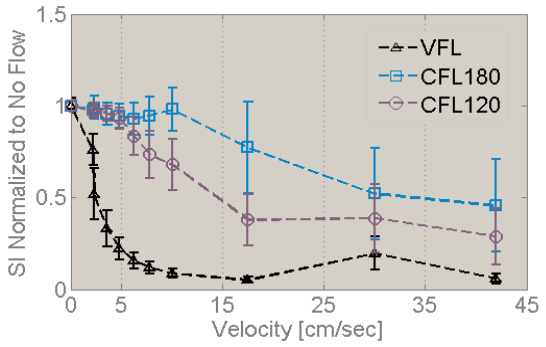

Figure 6.3. Relationship between flow velocity and signal intensity: phantom data

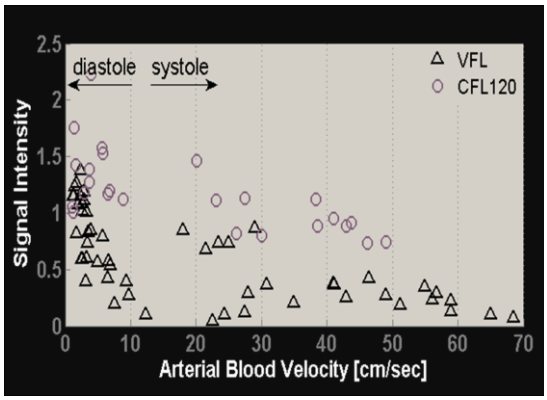

Figure 6.4. Relationship between flow velocity and signal intensity: *in vivo* data

6.1.3. Conclusion

Optimal arterial visualization with the ECG-gated fast spin echo is achieved when the difference between the systolic and diastolic arterial signal is maximized. Our results illustrated that arterial depiction depends on flow sensitivity, which in turn is tied to the flip angles used in the FSE echo train. With flow voids at velocities as low as 4-5 cm/sec, the VFL-approach we used is suboptimal for imaging vessels where diastolic flow exceeds this threshold. These initial findings motivated a more systematic study of how flow-sensitizing sequence parameters, flow velocity, and arterial depiction are related.

6.2. Theory

The loss of signal from moving protons in fast spin-echo imaging arises from two primary mechanisms: intravoxel dephasing from isochromats with different velocities, and mixing among pathways involving different combinations of spin echoes and stimulated echoes. If all

refocusing pulses in a fast spin-echo experiment have flip angles (FAs) of exactly 180°, the signal at each echo would be entirely governed by spin-echo pathways. However, it is common to use FAs of less than 180° to reduce specific absorption rate and to slow down signal decay of stationary tissues. This results in the formation of stimulated echoes. The phase evolution for moving protons undergoing stimulated echoes differs from that for spin echoes because of the time in which magnetization is stored along the longitudinal axis. There, it retains its phase memory but does not accumulate any additional phase. When stimulated and spin-echo pathways mix during echo formation, the difference in their motion-induced phases can cause signal loss. As the FA of the refocusing pulses determines the relative contributions of spin echoes and stimulated echoes, it strongly influences the flow sensitivity of the sequence.

6.3. Methods

6.3.1. Phantom Experiments

The effect of flip angle (FA) on signal intensity was measured over a range of flow speeds. Experiments were conducted at 3T on a Tim-TRIO system (Siemens, Erlangen, Germany) running VB13A software.

The phantom consisted of a displacement pump (CardioFlow, Shelley Medical Imaging Technologies, Toronto, Ontario, Canada) connected to a reservoir via braid-reinforced Tygon tubing (5/8″ inner diameter) to form a closed circuit. The pump was driven at constant flow rates of 0, 1, 2, 4, 6, 8, 12 and 16ml/s, which were selected to span the expected range of diastolic velocities in the popliteal artery. It was not considered necessary to include peak systolic velocities, since our experience has shown that the popliteal artery always appears dark in systole on fast spin-echo images. The circulating fluid in the flow phantom consisted of 3% glycerol in

water doped with 0.15ml/L Magnevist (gadopentetatedimeglumine, Bayer Healthcare Pharmaceuticals Inc, Wayne, NJ, USA) to approximate the relaxation times of blood. The pump was positioned outside the scan room and a loop of tubing was passed through a waveguide in the wall and into the scanner. There it was laid on the patient table to form two long straight sections parallel to the bore axis, about 17 cm apart, and connected by a loose turn. A small stationary phantom was placed between the two straight sections to provide additional coil loading. The entire arrangement was weighted down with sandbags to avoid motion, and covered with a body phased array coil, which was used in combination with spine coil elements in the patient table for signal reception. Scanner adjustments were performed once, at the beginning of the study, and the patient table remained fixed for the duration of the experiment.

A sample of the circulating fluid was drawn into a 35ml syringe to measure its relaxation times. T_1 and T_2 were measured at 3T using a segmented inversion-recovery sequence and a spin-echo sequence respectively. The inversion-recovery sequence consisted of a non-selective inversion pulse with a segmented low flip angle gradient-echo readout, which was repeated with several different inversion times. Sequence parameters were: TR = 20s, FA = 15°, BW = 260Hz/pixel, 5 lines per segment, in-plane voxel size 0.9mm × 0.9mm, slice thickness 8mm, TI = 40, 100, 200, 300, 500, 700, 1000, 1500, 2000, 3000, 5000 and 8000ms. The spin-echo sequence was repeated with several different echo times to measure T_2. Parameters were: TR = 10s, BW = 130Hz/pixel, in-plane voxel size 0.9mm × 0.9mm, slice thickness 8mm, TE = 12, 150, 300, 450 and 600ms.

Phase contrast imaging was used to measure the flow velocity in the tubing for each flow setting. Sequence parameters were: velocity-encoding factor (venc) = 60cm/s, in-plane voxel size 0.8mm × 0.8mm, axial slice perpendicular to the flow with slice thickness 5mm, BW =

391Hz/pixel, 5 lines per segment, FA/TE/TR = 20°/3.95ms/71.9ms (where TR includes all lines in a segment). Flow velocities at the center of the tubing were measured using Siemens Argus software.

The flow phantom was imaged using a 3D fast spin-echo sequence with non-selective excitation and refocusing pulses (Siemens product sequence 'tse_vfl'). The readout direction was chosen along the direction of flow. Sequence parameters were chosen to ensure that the results of the phantom experiments were relevant to the situation *in vivo*. To achieve a similar variation of signal with velocity, the readout gradients were required to have comparable strength and duration. This was done by using the same readout bandwidth as for the human studies (977Hz/pixel) and a similar resolution in the frequency-encoding direction (1.4mm, obtained with FOV = 350mm and a base resolution of 256). The echo spacing was 2.86ms, which fell within the range used in the human studies. The resolution in the phase-encoding direction was dictated by the need to mimic the degree of intravoxeldephasing that occurs *in vivo*. This meant having a similar ratio of lumen diameter to voxel size. We chose to model the popliteal artery, which has a lumen diameter of approximately 5 – 8mm in healthy subjects [69] and spans roughly 4 voxels (without interpolation) for typical imaging parameters *in vivo*. Given that the inner diameter of the tubing was 5/8″ (1.6cm), we chose a voxel width of 4mm in the phase-encoding direction (i.e. a phase resolution of 34%) for the phantom experiments. In the partition-encoding direction we used the minimum slice resolution (50%) in combination with a nominal slice thickness of 1mm.

Imaging of the phantom was performed without parallel imaging or partial Fourier sampling. Using the product fast spin-echo sequence with constant flip angle pulse trains, data were collected with nominal flip angles ranging from 60° (the minimum value) to 180° in steps

of 30°. For each flip angle, images were acquired with TE = 2.9ms (the minimum value) and 100ms. For TE = 100ms, the sequence was run with a repetition time of TR = 1400ms and 1 echo train per partition, giving an echo train duration of 200ms. For TE = 2.9ms it was run with TR = 700ms and 2 echo trains per partition, giving an echo train duration of 103ms. These choices ensured adequate dynamic range without saturating the signal. For the long TE acquisitions the phase-encoding order was linear, and for the short TE acquisitions it was centric, with positive and negative halves of k-space being sampled in alternate echo trains. Signal evaluation of the fast spin-echo images was performed by choosing regions of interest in the center of the tubing at the same level as that used for phase contrast imaging.

6.3.2. Human studies

The goal of the human studies was to investigate the effect of flip angle and echo time on the depiction of large and small arteries using the FBI technique, and thereby determine an optimal range of sequence parameters for imaging the calves.

Three healthy subjects participated in the study (two men, one woman, ages 23, 25 and 27). It was known from earlier exams that they represented a wide range of heart rates. All provided informed consent under an IRB-approved protocol, and each was imaged at 1.5T (Siemens Avanto with VB15A software) and 3T (Siemens Tim-TRIO with VB13A software). Peripheral phased array coils were used to image the calves in all studies except one. At the time of that study, the peripheral coil was not available, and two body phased array coils were used instead.

Phase contrast imaging was performed in an axial plane through the popliteal artery to measure the flow velocity time course and determine the trigger delay corresponding to peak

systolic flow. The table was positioned such that the imaging slice was at the center of the bore. This was done to ensure accuracy of the velocity-encoding gradients, since it is known that the magnetic fields produced by the gradient coils are nonlinear and the gradient amplitudes decrease far from isocenter. The sequence was run with retrospective ECG gating and the following parameters: venc = 100cm/s, in-plane voxel size 1.5mm × 1.5mm, slice thickness 5mm, 40 phases, BW = 391Hz/pixel, FA/TE/TR/lines per segment = 30°/3.53ms/40.7ms/3 at 1.5T and 20°/3.79ms/70.3ms/5 at 3T (where TR includes all lines in a segment).

Non-contrast MRA was performed using an ECG-gated 3D fast spin-echo sequence with non-selective excitation and refocusing pulses. Both constant flip angle and proton density weighted variable flip angle refocusing pulse trains were used. Two data sets were acquired within the same sequence, one during peak systolic flow, as determined by phase contrast imaging, and the other at end-diastole, with a trigger delay of zero. Using constant RF pulse trains, imaging was performed with flip angles ranging from 60° to 170° (the maximum being limited by SAR constraints). In addition, comparisons were made between short and long echo times (20 – 21ms and 83 – 109ms respectively). Echo times shorter than 20ms were not possible for these acquisitions because of the use of linear ordering in combination with partial Fourier phase sampling. The phase partial Fourier factor varied automatically with TE, reaching 100% at the longest echo time used (109ms). The acquisition window changed with TE, but fell within the range 118 – 216ms in all cases. Echo spacing was 2.86 – 2.96ms, depending on the choice of RF pulse length, a longer pulse being used at high flip angles to reduce SAR. Other parameters included: frequency-encoding direction head-foot, phase-encoding direction left-right, FOV = 400mm, base resolution 320, phase resolution 83 – 89%, 80 – 88 partitions with nominal slice thickness 1.5mm, slice resolution 75% and slice partial Fourier factor 6/8, BW = 977Hz/pixel,

GRAPPA acceleration factor 2 with 24 reference lines, data acquisition every R-R interval, restore pulse on, 2 echo trains per partition, and total acquisition time 180 – 198 heartbeats (depending on the number of partitions). Variable flip angle imaging was performed with an echo time of 7ms, echo spacing of 2.4ms, half-Fourier phase sampling and an acquisition window of 94 – 105ms. The shorter echo time compared to the constant flip angle acquisitions resulted from the use of centric ordering for the oversampled region at the center of k-space, and the shorter echo spacing was due to shorter RF pulses. Other parameters were as above.

6.4. Results

6.4.1. Phantom experiments

At 3T the relaxation times of the circulating fluid in the flow phantom were measured to be $T_1 = 2100 \pm 30$ ms and $T_2 = 232 \pm 1$ ms. These are comparable to the relaxation times of blood reported by Stanisz*et al.*[70], namely $T_1 = 1932 \pm 85$ and $T_2 = 275 \pm 50$ ms at 3T and $T_1 = 1441 \pm 120$ and $T_2 = 290 \pm 30$ ms at 1.5T.

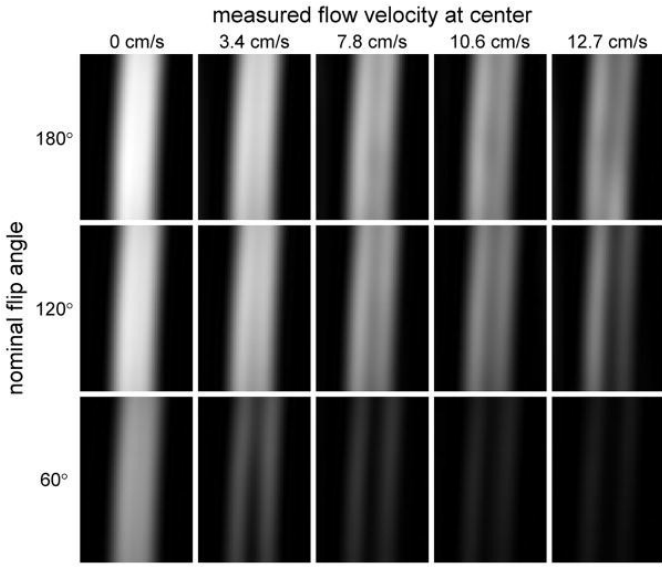

Figure 6.5. Cropped images of the flow phantom acquired using the product fast spin-echo sequence with constant flip angle refocusing pulses and TE = 100ms. Images are shown for three nominal flip angles (60°, 120° and 180°) and flow rates of 0, 4, 8, 12 and 16ml/s.

The flow velocities at the center of the tubing for flow rates of 1, 2, 4, 6, 8, 12 and 16ml/s were measured to be 0.95, 1.7, 3.4, 5.9, 7.8, 10.6 and 12.7 cm/s respectively. Figure 6.5 shows fast spin-echo images of the flow phantom for various flow rates and refocusing pulse flip angles, while Figure 6.6 displays the

signal intensities at the center of the tubing. Note that at zero flow velocity the intensities increase with flip angle. The absolute signal intensities (left graphs of Figure 6.5) should not, however, be compared between the two echo times since the acquisitions had different TR. For all parameter settings the signal intensities decrease as the flow velocity increases. The rate of decrease is a measure of the flow sensitivity, and is more easily compared across sequence parameters using the graphs of normalized signal (right). It can be seen that the flow sensitivity depends strongly on flip angle, increasing markedly as the flip angle decreases. At the lowest flip angle studied (60°), it appears that the flow sensitivity is greater for long TE than short TE, while at higher flip angles, the effect of TE on flow sensitivity is not significant.

For high flow rates and high flip angles, ghosts (i.e. replicas) of the tube lumen appeared at a distance of half the field of view in the phase-encoding direction (data not shown). Ghosting will be discussed further in the context of the human studies, where examples will be presented.

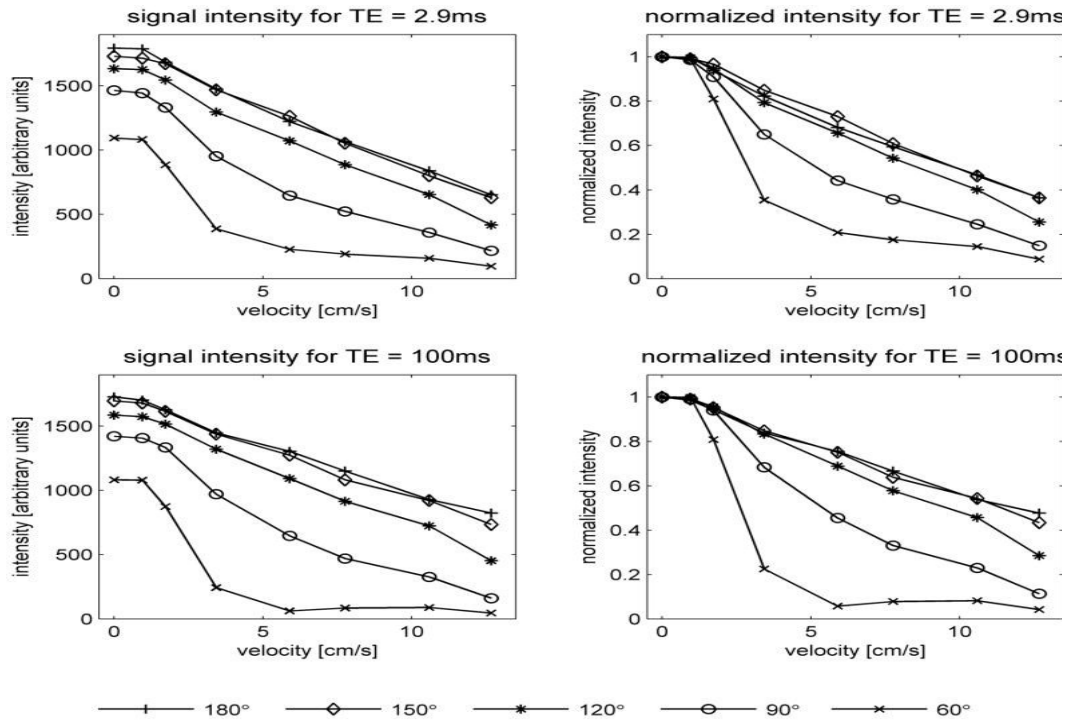

Figure 6.6. Signal intensities in the phantom as a function of flow velocity. Values were measured at the center of the tubing on images acquired using the product fast spin-echo sequence with constant flip angle pulse trains. Data are shown for nominal flip angles of 60°, 90°, 120°, 150° and 180°, and echo times of TE = 2.9ms (top) and TE = 100ms (bottom). The graphs on the left show absolute signal intensity, while those on the right show the signal intensity normalized to its value at zero flow. Absolute intensity should not be directly compared between the two echo times, since the acquisitions had different TR. Note that the flow sensitivity increases as the flip angle is reduced.

6.4.2. Human studies

In all subjects the flip angle of the refocusing pulses strongly affected the depiction of the arteries. Figure 6.7 shows results at 1.5T comparing different flip angles at a short echo time. In order to conserve space, only the right leg is shown. The large vessels (e.g. the popliteal artery and tibioperoneal trunk) are better depicted with a high flip angle; at low flip angles they exhibit signal loss at the center of the lumen. Inspection of the corresponding source images revealed low signal at the center of these vessels in diastole. This can be explained by the faster flow at the center of the vessel in combination with the greater flow sensitivity of the sequence for low flip angles, resulting in partial dephasing even in diastole. It should be pointed out that the

subject shown in Figure 6.7 had a relatively fast heart rate and high end-diastolic flow (93 ± 8 beats per minute and 6.7 ± 2.4 cm/s respectively, as recorded from phase contrast acquisitions on 3 separate days). The small branch vessels are better visualized at lower flip angle; at the highest flip angle tested (170°) many are not visible. Inspection of the source images for FA = 170° revealed high signal in these vessels in systole, suggesting that the peak flow velocities in the small branch arteries are not sufficient to cause dephasing at large flip angles.

At longer echo time (TE = 83ms, Figure 6.8) many of the same features are apparent; the larger vessels are better depicted at higher flip angle while the smaller vessels are better visualized at lower flip angle. One notable difference from the shorter echo time (c.f. Figure 6.7) is the greater signal loss at the center of the vessels for low flip angles. This suggests greater flow sensitivity at the longer echo time, in agreement with the results of the phantom experiments. Also, the signal profile of the popliteal artery appears slightly different between the two echo times, possibly due to differences in the point-spread function.

At the highest flip angle studied (170°) ghosts of the vessels occur in the phase-encoding direction (arrow). The distance between the ghosts is N/8 pixels, where N is the total number of pixels in the phase-encoding direction. Their appearance can be explained in terms of even-echo rephasing of spin-echo pathways, which causes a modulation of k-space in the phase-encoding direction. For our protocol, the modulation would have occurred with a period of 8 k-space lines, since we used an acceleration factor of 2 and acquired data over 2 echo trains per partition. This explains the distance of N/8 pixels between the ghosts in the image. The fact that they were not observed at lower flip angles is presumably because of the larger contribution of stimulated-echo pathways.

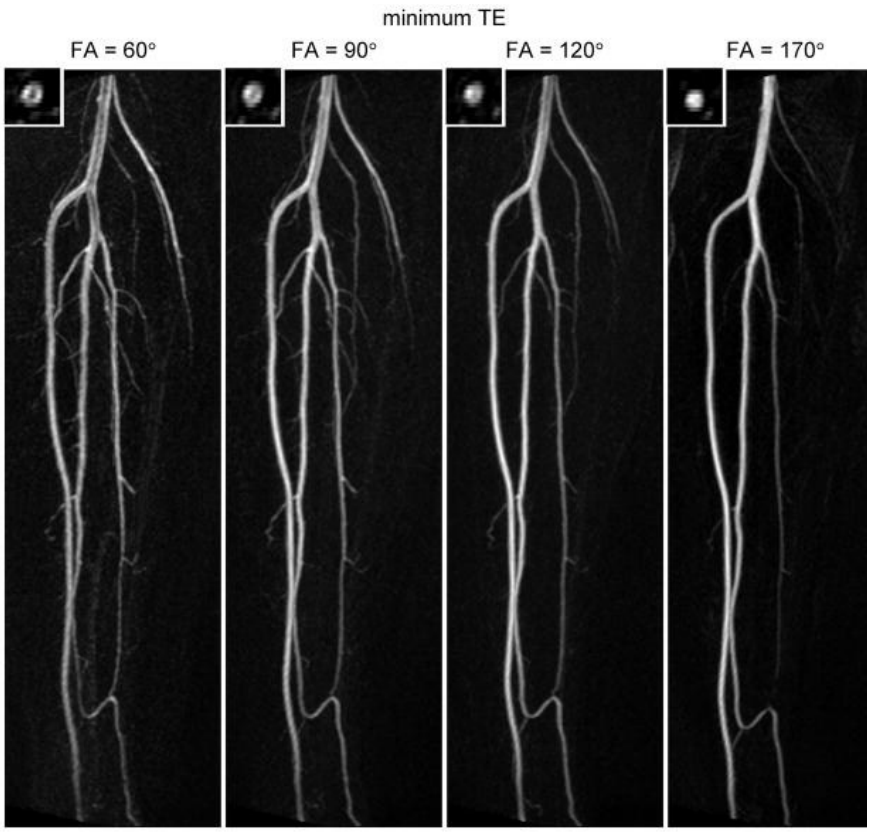

Figure 6.7. *In vivo* results in the right calf at 1.5T. Maximum intensity projections are shown for constant flip angle refocusing pulses of 60°, 90°, 120° and 170°. The echo time was set to its minimum value (TE = 20 ms for FA = 60°, 90° and 120°, and TE = 21ms for FA = 170°). The insets show axial cuts through the popliteal artery. Each image is individually windowed to use the full dynamic range. Note that the large vessels are better depicted at high flip angle, while the small branch vessels are better visualized at low flip angle.

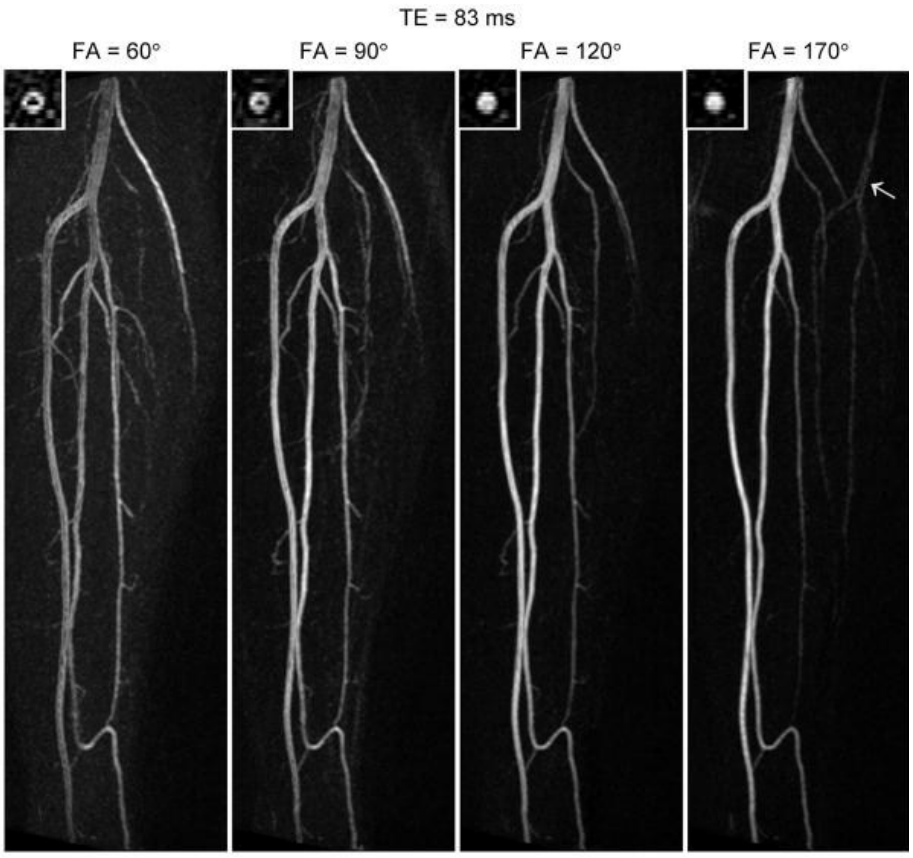

Figure 6.8. Maximum intensity projections acquired at 1.5T in the same subject as Figure 6.7, but with a longer echo time (TE = 83ms). The arrow in the image for 170° indicates an N/8 ghost (i.e. a replica of the vessel at a distance of N/8 pixels, where N is the number of pixels in the phase-encoding direction). Note that, for low flip angles, the signal loss is greater at the center of the popliteal artery in this figure (TE = 83ms) than in Figure 6.7 (TE = 20ms), suggesting a dependence of flow sensitivity on TE.

6.5. Discussion

In this chapter we examined the effect of flip angle and echo time on the flow sensitivity of ECG-FSE and the resultant depiction of the calf arteries. Our results demonstrate that FA is the most important determinant of flow sensitivity, with greater sensitivity to flow observed for lower FAs. Large arteries were better depicted with higher FAs, while small vessel branches benefited from lower FAs. In large vessels undesirable signal dephasing could occur in diastole

if the diastolic flow velocity is too high and the sequence is too flow sensitive. Conversely, small branches exhibit lower peak systolic velocities and their visualization may be compromised if the sequence is not sufficiently flow sensitive to provide adequate signal dephasing in systole.

End-diastolic and peak systolic velocities vary across subjects especially when pathology is present. The optimal degree of flow sensitivity is therefore subjected dependent. For example, less flow sensitivity may be preferable in the presence of hyperemia due to nonhealing wound, while greater flow sensitivity may be needed in patients with reduced cardiac output. Thus, tailoring the flow sensitivity of ECG-FSE via patient-depend selection of FA magnitude may achieve more robust image quality across patients and pathologies.

Although the number of people included in this study was low, the subjects spanned a wide range of heart rates. The optimal flip angles in this group lay in the range 90° – 120° and provided adequate depiction of large and small arteries in the calf. It is expected that a higher range of flip angles may be appropriate in the thigh, and that adjustments may be required in the presence of pathology. In practice, clinical history and phase contrast imaging through a large vessel could be used to determine qualitatively whether a subject has fast or slow flow compared to healthy controls. An appropriate flip angle could then be estimated with reference to the range given above. A rough estimate is expected to be adequate in most cases, since both large and small vessels are visualized over a fairly wide range of flip angles. If the initial estimate provided inadequate depiction of certain vessels, the flip angle could be adjusted appropriately and a second acquisition performed.

Further work will be needed to determine whether the sequence parameters considered in this study provide sufficient control of flow sensitivity to achieve adequate image quality in all relevant types of pathology. Other possibilities, such as the use of flow compensation, may need

to be explored. Alternative approaches to non-contrast MRA have been demonstrated that are less sensitive to the pulsatility of arterial flow or end-diastolic velocities. The flow-sensitive dephasing-prepared balanced SSFP technique [71] also involves subtraction of dark-artery systolic images from bright-artery diastolic images. However, the flow sensitivity is provided by a diffusion preparation module, which is applied only in systole. Thus the efficacy of the technique does not depend on end-diastolic velocities but only on peak systolic velocities. A new approach, Quiescent Interval Single-Shot (QISS) imaging [72], is an ECG-gated multislice 2D inflow-based technique, involving the application of traveling saturation bands to suppress background tissue and venous signal. Because of the relatively long quiescent period between the saturation pulses and the SSFP readout (228ms), even arteries with very slow flow can be visualized.

In conclusion, optimal performance of the fresh blood imaging technique depends on appropriate adjustment of the flow sensitivity of the underlying fast spin-echo sequence. The flow sensitivity is determined largely by the flip angle of the refocusing pulses and to a lesser extent by the echo time. These parameters should be tailored to the individual subject to achieve optimal depiction of the arterial system. It remains to be seen, however, whether they offer adequate control over flow sensitivity to provide accurate MR angiograms in other anatomic regions and in the presence of pathology [73, 74].

Chapter 7

Sagittal Fresh Blood Imaging with Interleaved Acquisition of Systole and Diastole for Improved Robustness to Motion

7.1 Introduction

"Fresh blood imaging" (FBI) [8], also known as ECG-FSE, has gained considerable popularity for non-contrast peripheral MRA. As described earlier, in this approach two sets of images are acquired, one in systole and one in diastole, with three-dimensional (3D) fast spin echo (FSE) sequence. Arteries appear bright in diastole when flow is slow, but darker in systole due to flow-induced signal dephasing. Bright-blood arterial angiograms are obtained by subtracting systolic from diastolic images.

Clinical evaluation of FBI in PAD patients, against either gadolinium-MRA or CT angiography [9-12, 54, 75], has demonstrated that the technique is susceptible to patient-induced motion artifacts with two studies reporting non-diagnostic results in as many as 47% [10, 75] of all cases. In FBI systolic and diastolic phase datasets are acquired sequentially, over the course of several minutes. Any motion between the two acquisitions can lead to subtraction errors due to misregistration, obscuring arteries on the difference image. One approach to improve tolerance to patient motion is to alternating between systolic and diastolic readouts at subsequent heart beats. This strategy would shorten the time window between corresponding systolic and diastolic acquisitions that need to be subtracted from 1-2 minutes to several seconds.

A foreseeable challenge for an interleaved FBI implementation is the resultant TR variation between subsequent readouts. Typically, FBI data is acquired every cardiac cycle, with

diastolic imaging performed at end-diastole with trigger delay (TD) of 0. Systolic datacollection occurs during peak-systole with a subject-specific TD, usually 200-300 ms after the R wave trigger. In a sequential regime, TR equals the duration of the cardiac cycle (1RR); however, in an interleaved acquisition, TR alternates between 1RR-TD and 1RR+TD leading to non-uniform T_1 relaxation of corresponding systolic and diastolic datasets.

Non-uniform TR may cause suboptimal depiction of small arteries and vessel edges. In an interleaved regime arterial signal is higher on diastolic images, while background tissue is brighter on systolic images due to a longer period of T_1 recovery prior to systolic readouts. This is potentially problematic for voxels that contain both background tissue and arterial lumen (e.g. near vessel edges or small arterial branches) where partial volume effects are at play. Upon subtraction of systolic from diastolic data, the positive difference in arterial signal in a given voxel may be canceled out by the negative difference in tissue signal within the same voxel. As a consequence, the artery would not be visible on the subtraction image. In addition to the partial volume effects, arterial depiction may be further compromised in vessel branches with minimal velocity. When flow-dephasing effects are negligible, the arterial signal difference between systole and diastole is primarily governed by T_1 relaxation. Thus, the longer T_1 recovery prior to systole may lead to lower diastolic arterial signal and subsequent cancelation of the artery upon subtraction.

Performing data collection every other heartbeat, or less frequently, can decrease the effect of non-uniform T_1 relaxation since the fractional difference between systolic and diastolic TR will be reduced. However, decreased acquisition frequency leads to increase in scan time. The trade-off between T_1 uniformity and scan time can be eliminated with the use of two (one for each leg) sagittally-oriented imaging slabs. Imaging in a sagittal plane substantially reduces

the size of the phase-encoding dimension, which allows acquiring more k-space lines per heartbeat, thereby permitting to image two sagittal slabs in the same scan time as one coronal. On the other hand, using two separate imaging slabs permits to alternate between the right and the left leg slabs at subsequent heart beats. As a result, if triggering takes place every heart beat, each extremity will have effective TR of ~ 2RR, allowing for prolonged T_1 recovery without scan time penalties.

The use of two imaging slabs also permits to set unique flow-sensitizing acquisition parametersfor each extremity, such as trigger delay and flip angle (FA) magnitude. This may be valuable when disease leads to flow asymmetry between the legs.

The objectives of this study were to demonstrate the feasibility of FBI with systole-diastole interleaving and two imaging slabs and to evaluate the robustness to motion of the proposed technique.

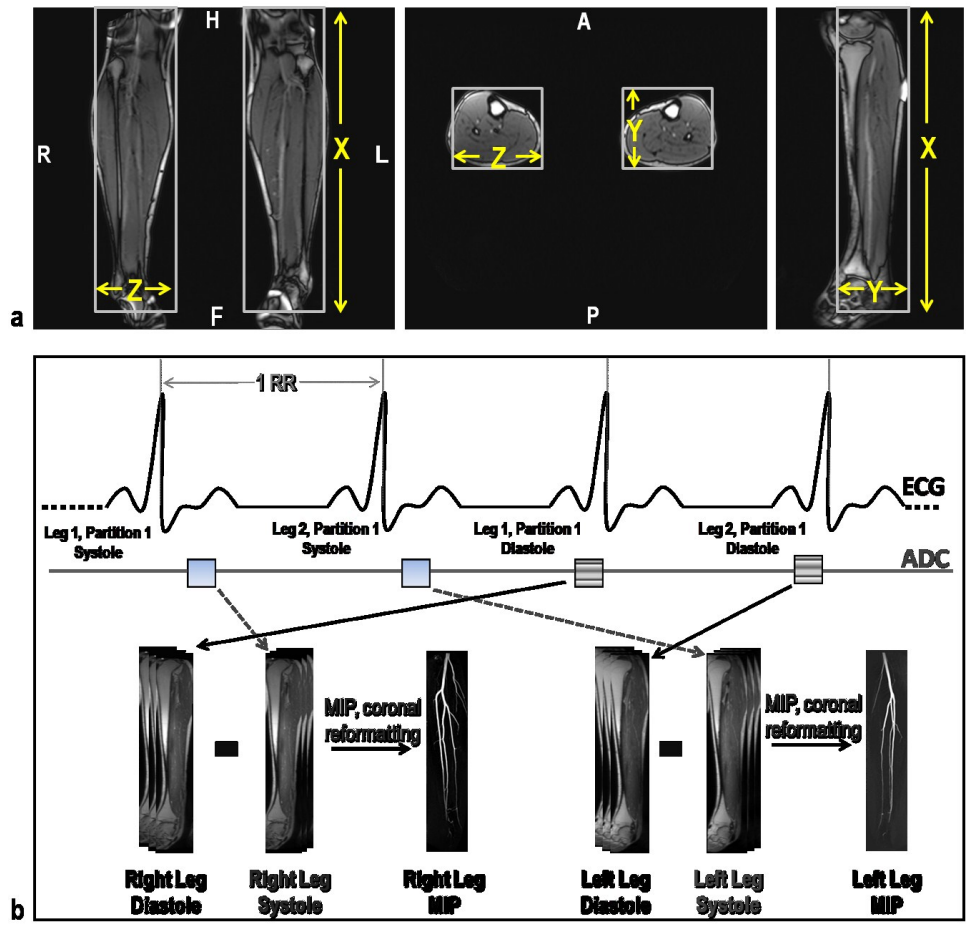

Figure 7.1.
(a) Image slab positioning. Interleaved-FBI uses two 3D imaging slabs, oriented sagittally, with frequency-encoding direction head-foot and phase-encoding direction anterior-posterior. (H = head, F = foot, R = right, L = left, A = anterior, P = posterior, X = frequency encoding direction, Y = phase encoding direction, Z = slice encoding direction).

(b) Sequence diagram. The readout is ECG-triggered and acquisition order alternates between left and right leg partitions at subsequent heartbeats. Imaging in a sagittal plane substantially reduces the size of the phase-encoding dimension and permits acquisition of a full k-space partition (entire k_x-k_y space per k_z) per heart beat and therefore enables imaging of two sagittal slabs in the same scan time as one coronal slab. Each extremity in interleaved-FBI is acquired with TR of approximately twice the TR of a sequential-FBI image obtained with identical acquisition frequency and scan

7.2 Materials and Methods

The distal lower extremities of 10 healthy volunteers (1 female, 9 male, age range 29 – 65 yrs; mean age 41 yrs), one volunteer with known PAD (male, age 72), and 3 patients (1 female, 2 male; age range 63 – 66yrs; mean age 63yrs) were imaged in this study. Patients were referred for contrast-enhanced MRA for suspected or known PAD. The study was approved by the Institutional Review Board, and written informed consent was obtained from all subjects. Imaging was performed on a whole-body 1.5T system (Avanto, Siemens Healthcare, Erlangen, Germany; maximum gradient strength = 45 mT/m; slew rate = 200 T/m/s). The body coil was used for radio-frequency excitation, while a 16-element peripheral matrix coil and a spine coil array were employed for signal reception.

7.2.1 Sequence

Interleaved-FBI uses two 3D imaging slabs, oriented sagittally, with frequency-encoding direction (k_x) head-foot, phase-encoding direction (k_y) anterior-posterior, and slice-encoding direction (k_z) right-left (Figure 7.1a). The 3D FSE acquisition is ECG-triggered and a full k-space partition (entire k_x-$k_y$space per k_z) is acquired per heartbeat. Acquisition order alternates between left and right leg partitions and between systolic and diastolic partitions (Figure 7.1b) as follows (assuming triggering every heart beat):

1. Cardiac cycle 1: right leg is excited for systolic data acquisition, after which $M_z$undergoes relaxation until cardiac cycle 3 for diastolic data acquisition
2. Cardiac cycle 2: left leg is excited for systolic data acquisition, after which M_z undergoes relaxation until cardiac cycle 4 for diastolic data acquisition

3. Cardiac cycle 3: right leg is excited for diastolic data acquisition, after which M_z undergoes relaxation until cardiac cycle 5 for systolic data acquisition
4. Cardiac cycle 4: left leg is excited for diastolic data acquisition, after which $M_z$undergoes relaxation until cardiac cycle 6 for systolic data acquisition

Right leg partitions acquired during the first and third cardiac cycles are subtracted, and similarly, left leg data obtained during heart beats 2 and 4 are subtracted. This read-out pattern is repeated until the full 3D volume of both imaging slabs is acquired.

When acquisition takes place every cardiac cycle $TR_{diastole}$ = 2*RR-TD, while $TR_{systole}$ = 2*RR+TD. To estimate the effect of non-uniform T_1 relaxation on slow vessel segments in this scenario, the difference in longitudinal magnetization ΔM_z between systolic and diastolic background as well as arterial signal was calculated as a function of M_0 for heart rates (HR) ranging 50 – 100 beats/min (bpm). We assumed complete signal loss following the readout and used a saturation recovery equation to calculate arterial and background M_z at the start of the subsequent excitation, using TD = 250 ms, arterial T_1 = 1200 ms[76], muscle T_1 = 1008 ms[70], flow velocity = 0 ms. For low heart rates ΔM_z was negligible (background ΔM_z= 0.05*$M_0$and arterial ΔM_z= 0.06*$M_0$for HR = 50 bpm) and exceed 1.5*M_0 for HR = 100 bpm. $\Delta M_z$of background muscle reached 0.1*M_0 at HR ~ 78 bpm, while arterial $\Delta M_z$was 0.1*M_0 at HR ~ 70 bpm. Based on these observations, we concluded that performing data acquisition every RR interval will be adequate in subjects with HR ≤ 80 bpm, while it may be necessary to image every other heart beat in patients with HR > 80 bpm.

7.2.2 Imaging Protocol

Acquisition parameters for 3D sequential FBI included: matrix size = 384x224x64, FOV = 500x375x96 mm^3, true voxel size 1.3x1.5x2.0 mm^3, BW 766 Hz/px, TE 19 ms, nonselective excitation andrefocusing pulses, echo spacing 3.3ms, echo train length 221 ms. Unless otherwise specified data collection was performed every cardiac cycle with GRAPPA factor of 1.8 and 2 shots per partition.

Interleaved FBI images were obtained with the following parameters: matrix size = 384x51x64, FOV = 500x101x96 mm^3, true voxel size 1.3x2.0x1.5 mm^3, BW 766 Hz/px, TE 20 ms, slice-selective excitation and refocusing pulses, echo spacing 5.0ms, echo train length 255 ms. Data collection was performed every cardiac cycle (unless noted otherwise) without acceleration and 1 shot per partition.

To perform a fair comparison between interleaved and sequential FBI, the sequences had identical voxel size in physical space; TE and read-out duration were also matched as closely as feasible. In both cases, diastolic TD was 0 ms; systolic TD was subject-specific as determined by cine MRI (axial plane through the popliteal artery, voxel size 1.6 x 1.6 mm^2, slice thickness = 6 mm, FA = 70°). The interleaved FBI sequence provided an option to input two systolic TDs, one for each leg. Based on prior *in vivo* experience [73, 77], the FA of the refocusing pulses was set to 120° in all subject. Interleaved FBI permitted to input a unique flip angle for each extremity. If asymmetric flow was suspected, phase contrast imaging (in-plane voxel size 1.5 × 1.5mm^2, slice thickness 5mm, venc = 90cm/s, FA = 30°.) was performed in an axial plane through the popliteal artery to measure the arterial flow velocity during the cardiac cycle and guide the selection of a lower or higher flip angle.

Following localization, TD, and velocity scout scans, three different MRA experiments were conducted:

Healthy volunteer scans with motion challenge: Ten healthy volunteers were imaged with both sequential and interleaved FBI while instructed to hold still. To test for tolerance to motion, these subjects underwent additional imaging during which they were periodically asked via the intercom to move their feet in a controlled manner. Four data sets with motion challenge were obtained per volunteer. First, subjects were asked to vigorously plantarflex and relax their toes 3-4 times, while being careful not to displace either extremity from its original position. Sequential and interleaved FBI were acquired, with the motion repeated every 30-40 seconds during image acquisition. Next, the volunteers were instructed to repeatedly externally rotate both feet 3 times at the ankle joint. The subjects were asked to return both extremities to their original position after the rotation. Again, the motion was repeated every 30-40 seconds during imaging with both techniques. To illustrate that interleaved FBI permits to image each extremity with a unique flip angle, one volunteer underwent an additional interleaved FBI scan, where the right leg flip angle was reduced to 60°.

Clinical comparison against Gd-MRA in patients: Three patients underwent sequential and interleaved FBI, followed by gadolinium-enhanced dynamic imaging of the calves and multi-station bolus-chase MRA. A total of 0.15 mmol/kg Gd-DTPA were injected, of which 0.04 mmol/kg were used for time-resolved imaging and 0.11 mmol/kg for bolus-chase.Timing was based on time-to-peak enhancement of the distal infrarenal aorta and a standard formula [62]. Dynamic imaging was performed with Time-resolved angiography With Interleaved Stochastic Trajectories (TWIST) and the following parameters: TR/TE 3.1/1.0ms, FA 25˚, nominal voxel size 1.0 mm x 1.3mm x 1.3 mm, slice resolution 93%. The distal station of the bolus-chase acquisition was performed with 3D T1-weighted Fast Low-Angle Shot (FLASH) sequence,

using: TR/TE 2.94/0.9 ms, FA 25˚, nominal voxel size 1.0 mm x 1.6mm x 1.4 mm, slice resolution 60%.

Effect of TR in a volunteer with known disease and fast heart rate: One volunteer with known PAD and fast heart rate was imaged with sequential and interleaved FBI, while instructed to hold still. Both sequences were run with data collection every cardiac cycle and repeated with prolonged TR, acquiring every other heart beat, in order to evaluate the effect of TR on arterial visualization.

7.2.3 Image Quality Assessment

All data were de-identified and randomized for blinded review by two radiologists who independently scored the images. Source, subtracted, and maximum intensity projection (MIP) images of all sequences were available to the readers; primary interpretation relied on the MIPs. Tenarterial segments per leg (popliteal, tibioperoneal trunk, proximal and distal anterior tibial artery, proximal and distal peroneal artery, proximal and distal posterior tibial artery, dorsalispedis, and plantar artery) were assessed for

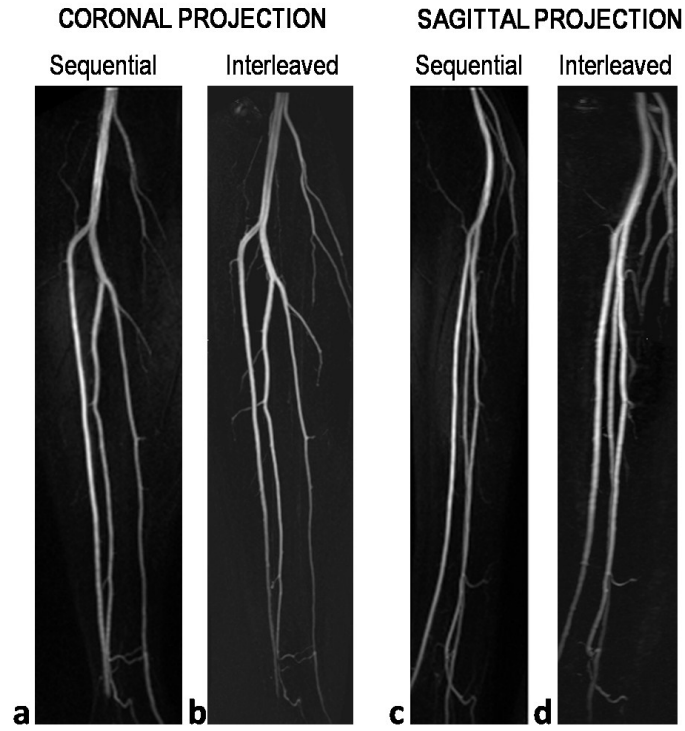

Figure 7.2. Right leg angiograms obtained in a 50 year-old male with heart rate = 60 bpm, instructed to hold still. The phase-encoding direction of the two sequences did not have the same physical orientation and resulted in different apparent vessel thickness on projection images. T2-blurring effects were more pronounced with sequential-FBI on coronal MIPs (a, b) and vice versa.

diagnostic quality on a 4-point scale (1 = non-diagnostic, 2 = poor, 3 = satisfactory, 4 = excellent).

7.2.4 Statistical Analysis

Image quality scores of all angiograms were averaged over the two readers and analyzed in Matlab. In healthy volunteers, Wilcoxon matched-pairs signed rank test was used to evaluate differences in arterial depiction between sequential and interleaved FBI for all three motion scenarios: still, toe flexion, and foot external rotation. In patients, the same test was used to compare both non-contrast sequences to Gd-MRA. In all tests, a P value < 0.05 was considered to be significant.

Figure 7.3. Right (a) and left (b) leg angiograms obtained in a 29 year-old male with heart rate = 72 bpm, instructed to hold still. The flexibility to use separate flow-sensitizing parameters for each leg may be valuable when pathology is present.

7.3 Results

7.3.1 Imaging at rest

Coronal and sagittal projections of interleaved and sequential FBI angiograms obtained in a healthy volunteer are displayed in Figure 7.2. On projection images, apparent vessel thickness differed between the two techniques as the phase-encoding direction of the interleaved and the sequential case did not have the same physical orientation. On coronal MIPs, T2-blurring effects were more pronounced with sequential-FBI, while on sagittal views the filtering effect was more apparent on interleaved-FBI images. Figure 7.3 displays interleaved FBI MRA with different flip angle settings for each leg. Using a lower flip angle for the left leg resulted in undesirable signal loss at the center of the popliteal artery, but better depiction of branch vessels.

In healthy volunteers, the two FBI versions had comparable quality when the subjects were instructed to hold still (Figure 7.4a, d). Overall image quality of interleaved FBI and sequential-FBI was excellent and averaged 3.78 ± 0.21and 3.60 ± 0.51 respectively on a scale of 1 to 4, where 4 is best. Similar results were obtained in the patient cohort, where both interleaved and sequential FBI exhibited image quality comparable to Gd-MRA. Image quality ratings obtained in volunteers and patients are summarized in Table 7.1. Among the patients, hemodynamicallysignificant disease was found in only one subject. In this case, disease was bilateral, but flow asymmetry between the legs, in terms of systolic peak timing and flow velocity, was not observed.

Figure 7.5 displays angiograms obtained in a 72 year old volunteer with PAD and heart rate 90 bpm. When cardiac triggering took place every RR (Figure7.5a, b), the right leg was better depicted with interleaved FBI due to patient motion artifacts on sequential FBI. Visualization of the left leg vasculature was poorer with interleaved FBI likely due to non-uniform T_1 relaxation combined with a short TR given the fast heart rate of the patient. When TR was doubled by triggering every other heart beat, sequential FBI (Figure 7.5c), resulted in a non-diagnostic image of the right leg and poor image quality of the left leg due to motion artifacts. Conversely, interleaved FBI (Figure 7.5d) exhibited excellent image quality and offered improved depiction of collateral flow compared to the case with shorter TR, owing to improved T_1 relaxation and reduced effect of non-uniform TR.

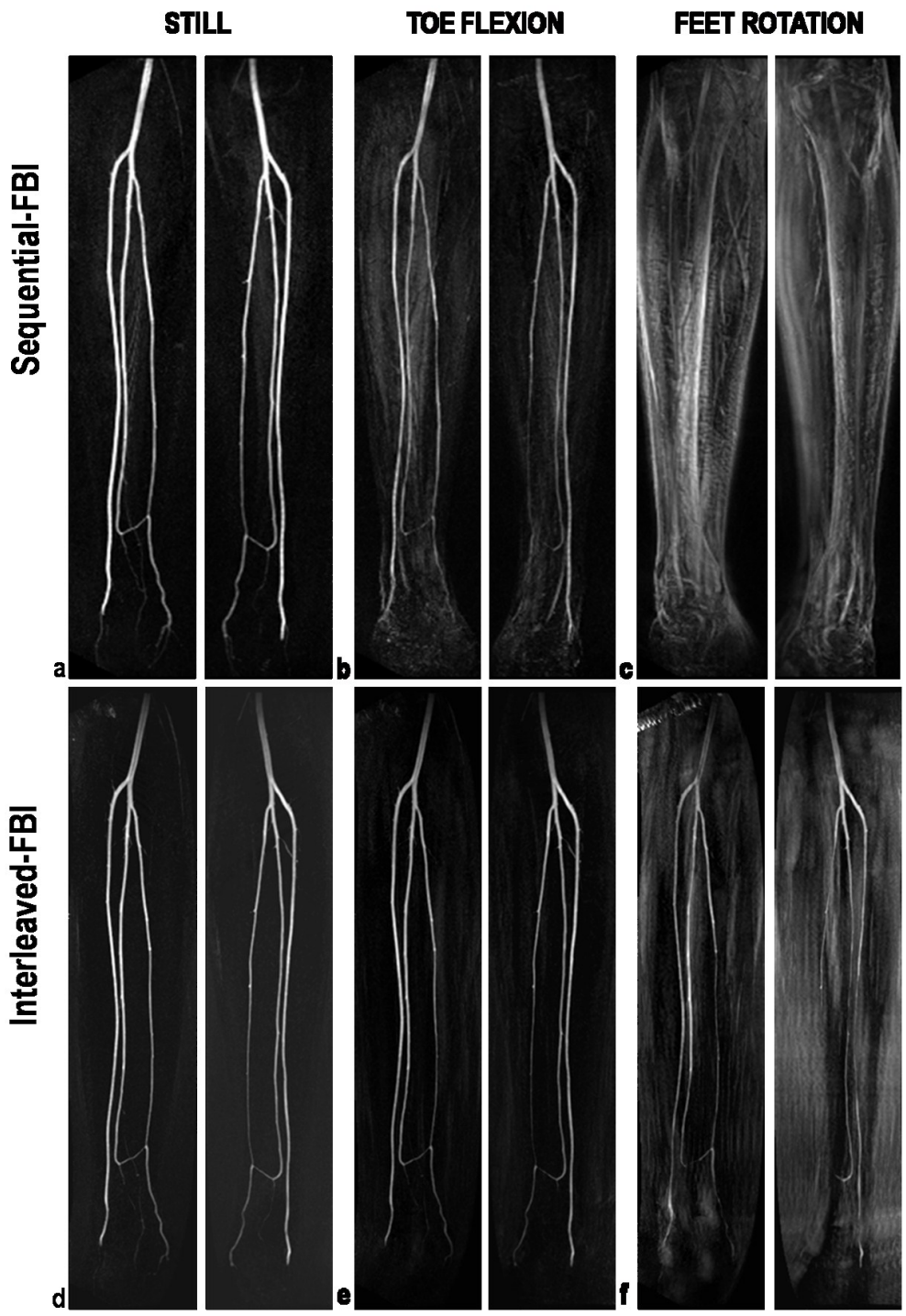

Figure 7.4. Comparison of interleaved-FBI and sequential-FBI for different motion scenarios in a 33 year old healthy subject. Interleaved-FBI offered improved tolerance to patient motion.

Sequence		Still	Toe flexion	Foot rotation
Volunteers	COR-FBI	3.60 ± 0.51	2.22 ± 1.01*	1.63 ± 0.78*
	SAG-FBI	3.78 ± 0.21	3.32 ± 0.74*	2.72 ± 0.72*
Patients	COR-FBI	3.73 ± 0.32		
	SAG-FBI	3.80 ± 0.26		
	Gd-MRA	3.90 ± 0.19		

Table 7.1.Image quality ratings of sequential-FBI and interleaved-FBI in 10 volunteers and 3 patients. * $p < 0.05$

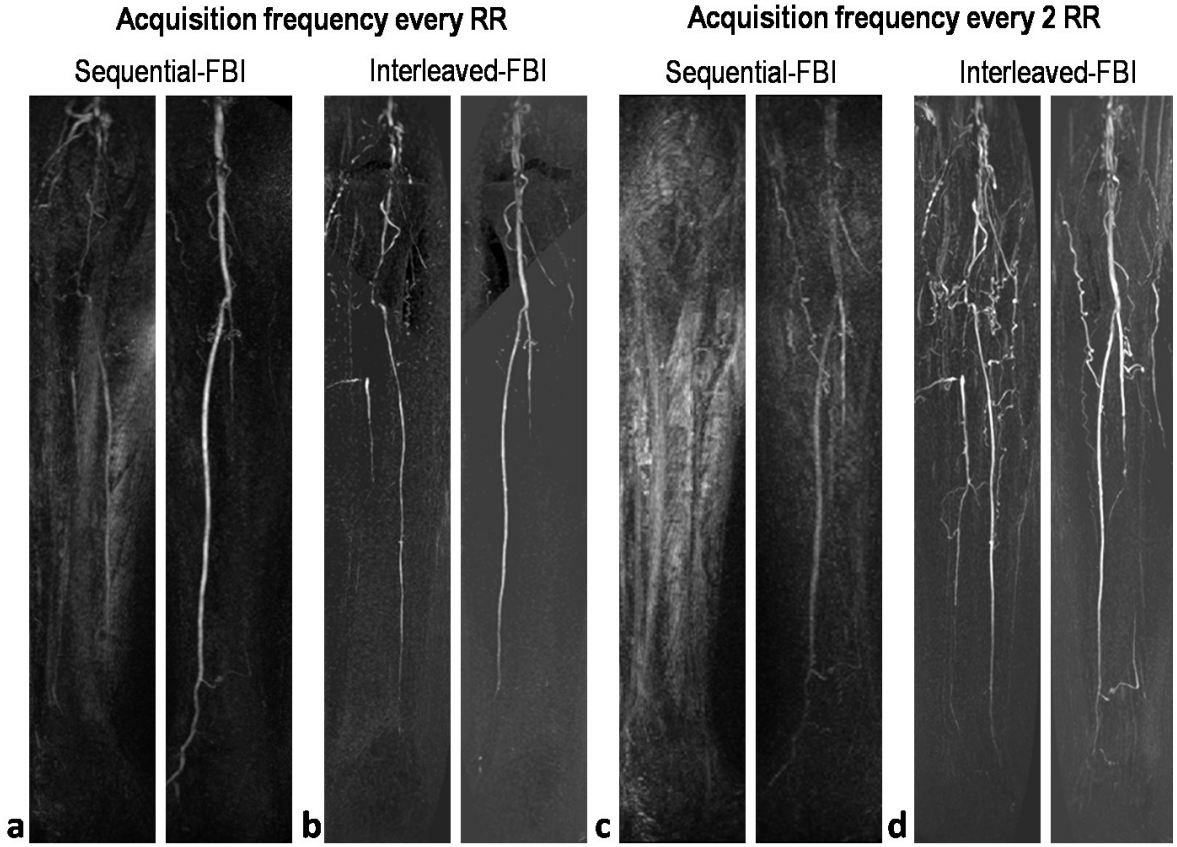

Figure 7.5. Interleaved-FBI and sequential-FBI angiograms obtained with data acquisition in a 72 year old volunteer with PAD and heart rate 90 bpm. When TR was doubled, sequential FBI resulted in a non-diagnostic image due to motion (c), while interleaved FBI (d) exhibited excellent image quality and offered improved depiction of collateral flow compared to the case with shorter TR due to improved T_1 recovery.

7.3.2 Imaging with motion challenge

In healthy volunteers, the image quality of both interleaved and sequential FBI deteriorated when deliberate motion was present; however, interleaved FBI received significantly higher quality scores. In the case of mild to moderate motion, i.e. toe flexion (Figure 7.4b, e), interleaved FBI produced image quality (3.32 ± 0.74)comparable to the motion-free scenario with no statistically significant differences found between the two, while sequential-FBI resulted in nearly poor ratings (2.22 ± 1.01). When severe motion (foot rotation) was present (Figure 7.4c, f), sequential-FBI produced non-diagnostic images in half of the volunteers with satisfactory or higher image quality observed in only 2 cases. In contrast, interleaved FBI was rated non-diagnostic in one volunteer, and satisfactory or better in 8 out of 10 cases.

7.4 Discussion

We have demonstrated that it is feasible to implement the FBI sequences with two sagittal imaging slabs and interleaved acquisition of systolic and diastolic partitions. In volunteers and patients imaged at rest, the modified FBI sequence produced excellent image quality, comparable to results obtained with sequential FBI and Gd-MRA. More importantly, our results indicate that the interleaved acquisition improves tolerance to patient motion. This is feasible due to shortening of the time window between the acquisition of corresponding systolic and diastolic partitions from 1 or 2 minutes in the sequential case to two cardiac cycles in the interleaved case. Better tolerance to patient motion may offer improved overall clinical performance of the FBI technique. It can also allow using longer scan times when severe disease is present and prolonged T_1 relaxation is necessary to visualize small-caliber collateral vessels (Figure7.5).

The use of separate imaging slabs for each extremity permits to use separate flow-sensitizing sequence parameters for each leg. Whether this flexibility improves the robustness of the technique to flow asymmetry requires evaluation in a larger clinical population. Differential flow was not observed in the small patient group imaged in this study and the potential benefits of parameter customization could not be assessed.

Systole-diastole interleaving with robust image quality and without scan time penalties was feasible owing to the use of two sagittal imaging slabs. Imaging in a sagittal plane reduces the size of the phase-encoding dimension, allowing for shorter acquisition windows which can be used to reduce T2-blurring or traded for time gains by acquiring more k-space lines per heart beat. In this work we pursued only the latter option. The smaller phase-encoding dimension of interleaved FBI permits to acquire two sagittal slabs as time-efficiently as one coronal, while the ability to alternate between right and left leg partitions allows prolonging the effective TR of each imaging slab without an increase in scan time.

In this study, the echo train duration of the sequential and the interleaved sequences were roughly identical. Interleaved FBI did not offer reduction in T2-blurring for two reasons. First, parallel imaging was not used for the sagittal scans because the orientation of the receiver coil elements did not permit for acceleration in the anterior-posterior direction, which coincided with the phase-encoding dimension of interleaved FBI. Second, sequential FBI is implemented with non-selective excitation and refocusing RF pulses to allow for shorter echo spacing and read-out duration. However, it is essential to use selective excitation and refocusing in interleaved FBI to avoid cross-excitation between the two imaging slabs. As a result, echo spacing of interleaved FBI was 5.0 ms compared to 3.3 ms for sequential-FBI. An implementation of the 3D FSE sequence with variable-rate selective excitation and refocusing pulses (VERSE) and echo

spacing shorter than 5.0 ms has been reported [78]. While T2-blurring considerations were beyond the scope of this work, interleaved FBI could be modified to allow for shorter echo train duration and reduced T2-blurring compared to sequential FBI.

Imaging patients with irregular or fast heart rates is a challenging aspect of both sequential and interleaved FBI. Rapid heart rates result in shortened TR intervals which may cause inadequate arterial signal difference between systole and diastole, particularly in vessel branches with low amounts of systolic flow-dephasing. Fast HR is especially problematic for interleaved FBI because it augments the effect of non-uniform TR between systole and diastole. Our theoretical considerations and *in vivo* experience with interleaved FBI indicate that triggering every second heart beat at the cost of increased scan time is necessary to ensure satisfactory image quality in patients with irregular or fast (> 80 bpm) heart rate.

In conclusion, a modification of the FBI sequence for non-contrast MRA of the distal lower extremities has been implemented to offer better robustness to patient motion and flow asymmetry. Initial results in volunteers, imaged while performing controlled movements, indicate improved tolerance to patient motion compared to the original technique. However, it is necessary to bear in mind that interleaved FBI is not a fool-proof solution against severe or constant motion. It remains to be studied whether the proposed modifications will improve the overall clinical performance FBI [79, 80].

Chapter 8

Conclusion

Non-contrast MRA techniques have been available since the early days of MRI, but until recently their clinical utility for peripheral angiography has been limited due to prohibitively long acquisition times. However, improvements in MRI hardware and software over the past decade have reduced acquisition times and made non-contrast imaging clinically practical. In 2003 a Japanese team led by Mitsue Miyazaki introduced the ECG-FSE sequence, extensively discussed in this manuscript, for lower extremity imaging. This invention was to an extent spurred by the high cost of gadolinium contrast in Japan. Around the same time, concerns about NSF in the USA led the FDA to advise against the use of Gd-MRA in patients with moderate to severe end-stage renal disease, creating an unmet clinical need for contrast-free imaging techniques.

Several clinical sites in the USA and Europe have tested ECG-FSE; however, to this date, widespread clinical adoption of the technique has not occurred due to serious technical limitations. This thesis described two studies aimed at improving the clinical performance of ECG-FSE in the lower extremities. First, the relationship between FSE flip angle magnitude and arterial visualization was investigated. It is anticipated that improved understanding of how sequence parameters affect image quality would be useful for optimization of clinical protocols. Second, the implementation of ECG-FSE was modified to allow interleaving of systolic and diastolic data acquisition. Preliminary results in volunteers suggest that the proposed modification offers improved robustness to patient motion. It remains to be studied whether the findings reported in this thesis will improve the overall clinical performance of ECG-FSE.

Peripheral MRA exams require visualization of both the slower-flowing arteries of the lower extremities and the faster-flowing vessels of the abdomen and pelvis. While ECG-FSE is well-suited for imaging of slow-flow vessels, the physical principle of the sequence is violated in the abdomen where diastolic velocities of the arteries are non-zero. For that reason, the development of a non-contrast technique suitable for abdominopelvic imaging was a primary focus of this dissertation. Robust unenhanced MRA techniques, based on arterial inflow, have been developed for visualization of the renal arteries as a complement to Gd-MRA due to poor visualization of the distal renal artery branches on Gd-MRA. Here the concept of inflow-based renal MRA was extended for large FOV visualization of the entire abdomen without contrast injection.

Combining the optimized ECG-FSE sequence and the new abdominal technique into a hybrid peripheral MRA protocol permits non-contrast visualization of the arterial tree from renal to pedal arteries. Investigation in a large patient cohort is necessary to validate whether the protocol proposed here is a robust alternative to Gd-MRA.

During the course of this dissertation two alternative non-contrast techniques for peripheral MRA were developed elsewhere. Flow-sensitive dephasing prepared b-SSFP (FSD-MRA) is a subtraction technique that, similarly to ECG-FSE, relies on arterial flow velocity variations during the cardiac cycle [71]. Arterial signal voids are obtained in systole via an FSD preparation module applied prior to the readout to induce signal dephasing. Feasibility of calf imaging with FSD-MRA has been demonstrated; however, thorough evaluation of the method in a clinical population has not been reported yet. Quiescent-Interval Single-Shot (QISS) MRA is the most recently introduced non-contrast MRA technique, based on a 2D TOF principle [72]. To date, QISS has been evaluated in a three clinical studies with reported sensitivity and specificity

values consistently above 95% [81, 82]. Given the current clinical evidence, QISS is by far the most reliable non-contrast peripheral MRA method in existence today, but wider clinical adoption would require more extensive clinical trials.

While various non-contrast alternatives for peripheral MRA exist, none have matched the reliability of Gd-MRA in terms of speed and technical robustness, and routine clinical practice in the USA nowadays relies primarily on contrast-enhanced MRA. NC MRA may never become the first-line imaging option for peripheral MRA, but robust alternatives to Gd-MRA are clinically needed for the growing population of patients with coexisting PAD and renal insufficiency.

The main limitation of most non-contrast techniques is their reliance on the flow dynamics of the imaged vessels, making it challenging, if not impossible, to tailor the sequence parameters to numerous unique flow patterns caused by pathology. The need for cardiac or respiratory triggering is another limitation which renders most techniques prone to artifacts in patients with arrhythmias and irregular breathing patterns. The non-contrast MRA sequence of the future will be fast, flow-independent, free of ECG and respiratory triggering, and will be able to provide time-resolved information about flow dynamics.

REFERENCES

1. Sigvant B, Wiberg-Hedman K, Bergqvist D, Rolandsson O, Andersson B, Persson E, Wahlberg E: **A population-based study of peripheral arterial disease prevalence with special focus on critical limb ischemia and sex differences**. *J Vasc Surg* 2007, **45**(6):1185-1191.

2. Norgren L, Hiatt WR, Dormandy JA, Nehler MR, Harris KA, Fowkes FG, Bell K, Caporusso J, Durand-Zaleski I, Komori K *et al*: **Inter-Society Consensus for the Management of Peripheral Arterial Disease (TASC II)**. *Eur J Vasc Endovasc Surg* 2007, **33 Suppl 1**:S1-75.

3. Ouriel K: **Peripheral arterial disease**. *Lancet* 2001, **358**(9289):1257-1264.

4. O'Donnell ME, Reid JA, Lau LL, Hannon RJ, Lee B: **Optimal management of peripheral arterial disease for the non-specialist**. *Ulster Med J*, **80**(1):33-41.

5. Sadowski EA, Bennett LK, Chan MR, Wentland AL, Garrett AL, Garrett RW, Djamali A: **Nephrogenic systemic fibrosis: risk factors and incidence estimation**. *Radiology* 2007, **243**(1):148-157.

6. Hoppe H, Spagnuolo S, Froehlich JM, Nievergelt H, Dinkel HP, Gretener S, Thoeny HC: **Retrospective analysis of patients for development of nephrogenic systemic fibrosis following conventional angiography using gadolinium-based contrast agents**. *European radiology* 2010, **20**(3):595-603.

7. Paraskevas KI, Giannoukas AD, Mikhailidis DP: **Renal function impairment in peripheral arterial disease: an important parameter that should not be neglected**. *Annals of vascular surgery* 2009, **23**(5):690-699.

8. Miyazaki M, Takai H, Sugiura S, Wada H, Kuwahara R, Urata J: **Peripheral MR angiography: separation of arteries from veins with flow-spoiled gradient pulses in electrocardiography-triggered three-dimensional half-Fourier fast spin-echo imaging**. *Radiology* 2003, **227**(3):890-896.

9. Gutzeit A, Sutter R, Froehlich JM, Roos JE, Sautter T, Schoch E, Giger B, Wyss M, Graf N, von Weymarn C *et al*: **ECG-triggered non-contrast-enhanced MR angiography (TRANCE) versus digital subtraction angiography (DSA) in patients with peripheral arterial occlusive disease of the lower extremities**. *European radiology* 2011, **21**(9):1979-1987.

10. Lim RP, Hecht EM, Xu J, Babb JS, Oesingmann N, Wong S, Muhs BE, Gagne P, Lee VS: **3D nongadolinium-enhanced ECG-gated MRA of the distal lower extremities: preliminary clinical experience**. *Journal of magnetic resonance imaging : JMRI* 2008, **28**(1):181-189.

11. Nakamura K, Miyazaki M, Kuroki K, Yamamoto A, Hiramine A, Admiraal-Behloul F: **Noncontrast-enhanced peripheral MRA: technical optimization of flow-spoiled fresh blood imaging for screening peripheral arterial diseases**. *Magn Reson Med*, **65**(2):595-602.

12. Mohrs OK, Petersen SE, Heidt MC, Schulze T, Schmitt P, Bergemann S, Kauczor HU: **High-resolution 3D non-contrast-enhanced, ECG-gated, multi-step MR angiography of the lower extremities: comparison with contrast-enhanced MR angiography**. *European radiology* 2011, **21**(2):434-442.

13. Katoh M, Buecker A, Stuber M, Gunther RW, Spuentrup E: **Free-breathing renal MR angiography with steady-state free-precession (SSFP) and slab-selective spin inversion: initial results**. *Kidney international* 2004, **66**(3):1272-1278.

14. Wyttenbach R, Braghetti A, Wyss M, Alerci M, Briner L, Santini P, Cozzi L, Di Valentino M, Katoh M, Marone C *et al*: **Renal artery assessment with nonenhanced steady-state free precession versus contrast-enhanced MR angiography**. *Radiology* 2007, **245**(1):186-195.

15. Herborn CU, Watkins DM, Runge VM, Gendron JM, Montgomery ML, Naul LG: **Renal arteries: comparison of steady-state free precession MR angiography and contrast-enhanced MR angiography**. *Radiology* 2006, **239**(1):263-268.

16. Maki JH, Wilson GJ, Eubank WB, Glickerman DJ, Millan JA, Hoogeveen RM: **Navigator-gated MR angiography of the renal arteries: a potential screening tool for renal artery stenosis**. *AJR American journal of roentgenology* 2007, **188**(6):W540-546.

17. Glockner JF, Takahashi N, Kawashima A, Woodrum DA, Stanley DW, Takei N, Miyoshi M, Sun W: **Non-contrast renal artery MRA using an inflow inversion recovery steady state free precession technique (Inhance): comparison with 3D contrast-enhanced MRA**. *Journal of magnetic resonance imaging : JMRI* 2010, **31**(6):1411-1418.

18. Luther M, Lepantalo M, Alback A, Matzke S: **Amputation rates as a measure of vascular surgical results**. *Br J Surg* 1996, **83**(2):241-244.

19. Roger VL, Go AS, Lloyd-Jones DM, Benjamin EJ, Berry JD, Borden WB, Bravata DM, Dai S, Ford ES, Fox CS *et al*: **Heart disease and stroke statistics--2012 update: a report from the American Heart Association**. *Circulation*, **125**(1):e2-e220.

20. Hankey GJ, Norman PE, Eikelboom JW: **Medical treatment of peripheral arterial disease**. *JAMA* 2006, **295**(5):547-553.

21. Murabito JM, D'Agostino RB, Silbershatz H, Wilson WF: **Intermittent claudication. A risk profile from The Framingham Heart Study**. *Circulation* 1997, **96**(1):44-49.

22. Willigendael EM, Teijink JA, Bartelink ML, Kuiken BW, Boiten J, Moll FL, Buller HR, Prins MH: **Influence of smoking on incidence and prevalence of peripheral arterial disease**. *J Vasc Surg* 2004, **40**(6):1158-1165.

23. Ingolfsson IO, Sigurdsson G, Sigvaldason H, Thorgeirsson G, Sigfusson N: **A marked decline in the prevalence and incidence of intermittent claudication in Icelandic men 1968-1986: a strong relationship to smoking and serum cholesterol--the Reykjavik Study**. *J Clin Epidemiol* 1994, **47**(11):1237-1243.

24. Zimmerman BR, Palumbo PJ, O'Fallon WM, Ellefson RD, Osmundson PJ, Kazmier FJ: **A prospective study of peripheral occlusive arterial disease in diabetes. III. Initial lipid and lipoprotein findings**. *Mayo Clin Proc* 1981, **56**(4):233-242.

25. Kreines K, Johnson E, Albrink M, Knatterud GL, Levin ME, Lewitan A, Newberry W, Rose FA: **The course of peripheral vascular disease in non-insulin-dependent diabetes**. *Diabetes Care* 1985, **8**(3):235-243.

26. Newman AB, Sutton-Tyrrell K, Vogt MT, Kuller LH: **Morbidity and mortality in hypertensive adults with a low ankle/arm blood pressure index**. *JAMA* 1993, **270**(4):487-489.

27. **Executive Summary of The Third Report of The National Cholesterol Education Program (NCEP) Expert Panel on Detection, Evaluation, And Treatment of High Blood Cholesterol In Adults (Adult Treatment Panel III)**. *JAMA* 2001, **285**(19):2486-2497.

28. Sharma M, Rai SK, Tiwari M, Chandra R: **Effect of hyperhomocysteinemia on cardiovascular risk factors and initiation of atherosclerosis in Wistar rats**. *Eur J Pharmacol* 2007, **574**(1):49-60.

29. Clarke R, Daly L, Robinson K, Naughten E, Cahalane S, Fowler B, Graham I: **Hyperhomocysteinemia: an independent risk factor for vascular disease**. *N Engl J Med* 1991, **324**(17):1149-1155.

30. Chan D, Anderson ME, Dolmatch BL: **Imaging evaluation of lower extremity infrainguinal disease: role of the noninvasive vascular laboratory, computed tomography angiography, and magnetic resonance angiography**. *Tech Vasc Interv Radiol*, **13**(1):11-22.

31. Reimer P, Landwehr P: **Non-invasive vascular imaging of peripheral vessels**. *European radiology* 1998, **8**(6):858-872.

32. Borrello JA: **MR angiography versus conventional X-ray angiography in the lower extremities: everyone wins**. *Radiology* 1993, **187**(3):615-617.

33. Singri N, Ahya SN, Levin ML: **Acute renal failure**. *JAMA* 2003, **289**(6):747-751.

34. Liistro F, Falsini G, Bolognese L: **The clinical burden of contrast media-induced nephropathy**. *Ital Heart J* 2003, **4**(10):668-676.

35. Sun Z: **Diagnostic accuracy of multislice CT angiography in peripheral arterial disease**. *J Vasc Interv Radiol* 2006, **17**(12):1915-1921.

36. Miyazaki M, Lee VS: **Nonenhanced MR angiography**. *Radiology* 2008, **248**(1):20-43.

37. Donald W. McRobbie EAM, Martin J. Graves, and Martin R. Prince: **MRI From Picture to Proton**, 2nd edn. New York, NY: CAMBRIDGE UNIVERSITY PRESS; 2006.

38. Prince MR: **Gadolinium-enhanced MR aortography**. *Radiology* 1994, **191**(1):155-164.

39. Heidrich H: **Frequency of non-vascular accompanying diseases in patients with peripheral arterial disease**. *VASA Zeitschrift fur Gefasskrankheiten Journal for vascular diseases* 2004, **33**(3):155-158.

40. O'Hare AM, Bertenthal D, Shlipak MG, Sen S, Chren MM: **Impact of renal insufficiency on mortality in advanced lower extremity peripheral arterial disease**. *Journal of the American Society of Nephrology : JASN* 2005, **16**(2):514-519.

41. Cowper S: **Nephrogenic Systemic Fibrosis**. In: *[ICNSFR Website].* 2011.

42. Kuo PH, Kanal E, Abu-Alfa AK, Cowper SE: **Gadolinium-based MR contrast agents and nephrogenic systemic fibrosis**. *Radiology* 2007, **242**(3):647-649.

43. Aydingoz U: **The need for radiologists' awareness of nephrogenic systemic fibrosis**. *Diagn Interv Radiol* 2006, **12**(4):161-162.

44. Grobner T: **Gadolinium--a specific trigger for the development of nephrogenic fibrosing dermopathy and nephrogenic systemic fibrosis?** *Nephrol Dial Transplant* 2006, **21**(4):1104-1108.

45. Marckmann P, Skov L, Rossen K, Dupont A, Damholt MB, Heaf JG, Thomsen HS: **Nephrogenic systemic fibrosis: suspected causative role of gadodiamide used for contrast-enhanced magnetic resonance imaging**. *Journal of the American Society of Nephrology : JASN* 2006, **17**(9):2359-2362.

46. Thomsen HS, Morcos SK, Dawson P: **Is there a causal relation between the administration of gadolinium based contrast media and the development of nephrogenic systemic fibrosis (NSF)?** *Clin Radiol* 2006, **61**(11):905-906.

47. USFaD A: **Public health advisory: gadolinium-containing contrast agents for magnetic resonance imaging (MRI)--Omniscan, OptiMARK, Magnevist, ProHance, and MultiHance.** June 8, 2006.

48. Kanal E, Barkovich AJ, Bell C, Borgstede JP, Bradley WG, Jr., Froelich JW, Gilk T, Gimbel JR, Gosbee J, Kuhni-Kaminski E *et al*: **ACR guidance document for safe MR practices: 2007**. *AJR American journal of roentgenology* 2007, **188**(6):1447-1474.

49. EAftEoM. P: **Gadolinium-containing MRI contrast agents and Nephrogenic Systemic Fibrosis (NSF)**. *In London* 2007.

50. Scheffler K, Lehnhardt S: **Principles and applications of balanced SSFP techniques**. *European radiology* 2003, **13**(11):2409-2418.

51. Miyazaki M, Isoda H: **Non-contrast-enhanced MR angiography of the abdomen**. *Eur J Radiol*, **80**(1):9-23.

52. Brittain JH, Olcott EW, Szuba A, Gold GE, Wright GA, Irarrazaval P, Nishimura DG: **Three-dimensional flow-independent peripheral angiography**. *Magn Reson Med* 1997, **38**(3):343-354.

53. Wedeen VJ, Meuli RA, Edelman RR, Geller SC, Frank LR, Brady TJ, Rosen BR: **Projective imaging of pulsatile flow with magnetic resonance**. *Science* 1985, **230**(4728):946-948.

54. Li D, Lin J, Yan F, Wu Q, Lv W, San Y, Yun H: **Unenhanced calf MR angiography at 3.0 T using electrocardiography-gated partial-fourier fast spin echo imaging with variable flip angle**. *European radiology*, **21**(6):1311-1322.

55. Atanasova IP, Kim D, Lim RP, Storey P, Kim S, Guo H, Lee VS: **Noncontrast MR angiography for comprehensive assessment of abdominopelvic arteries using quadruple inversion-recovery preconditioning and 3D balanced steady-state free precession imaging**. *Journal of magnetic resonance imaging : JMRI* 2011, **33**(6):1430-1439.

56. Liu X, Berg N, Sheehan J, Bi X, Weale P, Jerecic R, Carr J: **Renal transplant: nonenhanced renal MR angiography with magnetization-prepared steady-state free precession**. *Radiology* 2009, **251**(2):535-542.

57. Shonai T, Takahashi T, Ikeguchi H, Miyazaki M, Amano K, Yui M: **Improved arterial visibility using short-tau inversion-recovery (STIR) fat suppression in non-contrast-enhanced time-spatial labeling inversion pulse (Time-SLIP) renal MR angiography (MRA)**. *Journal of magnetic resonance imaging : JMRI* 2009, **29**(6):1471-1477.

58. de Bazelaire CM, Duhamel GD, Rofsky NM, Alsop DC: **MR imaging relaxation times of abdominal and pelvic tissues measured in vivo at 3.0 T: preliminary results**. *Radiology* 2004, **230**(3):652-659.

59. Gold GE, Han E, Stainsby J, Wright G, Brittain J, Beaulieu C: **Musculoskeletal MRI at 3.0 T: relaxation times and image contrast**. *AJR Am J Roentgenol* 2004, **183**(2):343-351.

60. Parker DL, Tsuruda JS, Goodrich KC, Alexander AL, Buswell HR: **Contrast-enhanced magnetic resonance angiography of cerebral arteries. A review**. *Invest Radiol* 1998, **33**(9):560-572.

61. Griswold MA, Jakob PM, Heidemann RM, Nittka M, Jellus V, Wang J, Kiefer B, Haase A: **Generalized autocalibrating partially parallel acquisitions (GRAPPA)**. *Magn Reson Med* 2002, **47**(6):1202-1210.

62. Earls JP, Rofsky NM, DeCorato DR, Krinsky GA, Weinreb JC: **Breath-hold single-dose gadolinium-enhanced three-dimensional MR aortography: usefulness of a timing examination and MR power injector**. *Radiology* 1996, **201**(3):705-710.

63. Zech CJ, Herrmann KA, Huber A, Dietrich O, Stemmer A, Herzog P, Reiser MF, Schoenberg SO: **High-resolution MR-imaging of the liver with T2-weighted sequences using integrated parallel imaging: comparison of prospective motion correction and respiratory triggering**. *J Magn Reson Imaging* 2004, **20**(3):443-450.

64. Saranathan M BE, Glockner J: **Group-encoded Ungated Inversion Nulling for Non-contrast Enhancement in the Steady State (GUINNESS): a balanced SSFP-Dixon technique for breath-held non-contrast MRA**. In: *18th Annual Meeting of ISMRM: 2010; Stockholm, Sweden*; 2010.

65. Takei N SM, Miyoshi M, Tsukamoto T: **Breathhold inhance inflow IR (BH-IFIR) with a novel 3D recessed fan beam view ordering**. In: *18th Annual Meeting of ISMRM: 2010; Stockholm, Sweden*; 2010.

66. Atanasova IP, Kim D, Lim RP, Storey P, Kim S, Lee VS: **Noncontrast MR angiography for comprehensive assessment of abdominoplevic arteries using quadruple inversion-recovery preconditioning and 3D balanced steady-state free precession imaging**. *Proc Intl Soc Mag Reson Med* 2011:3348.

67. Atanasova IP, Lim RP, Chandarana H, Stoffel D, Bruno M, Kim D, Lee VS: **Clinical validation of non-contrast abdominal MRA with quadruple inversion-recovery prepared 3D b-SSFP**. *Proc Intl Soc Mag Reson Med* 2012:3348.

68. Mugler JP WL, Brookeman JR: **T2-weighted 3D spin-echo train imaging of the brain at 3 tesla: reduced power deposition using low flip-angle refocusing RF pulses**. *Proc Intl Soc Mag Reson Med 2001* 2001, **9:438**.

69. Sandgren T, Sonesson B, Ahlgren AR, Lanne T: **Factors predicting the diameter of the popliteal artery in healthy humans**. *J Vasc Surg* 1998, **28**(2):284-289.

70. Stanisz GJ, Odrobina EE, Pun J, Escaravage M, Graham SJ, Bronskill MJ, Henkelman RM: **T1, T2 relaxation and magnetization transfer in tissue at 3T**. *Magn Reson Med* 2005, **54**(3):507-512.

71. Fan Z, Sheehan J, Bi X, Liu X, Carr J, Li D: **3D noncontrast MR angiography of the distal lower extremities using flow-sensitive dephasing (FSD)-prepared balanced SSFP**. *Magn Reson Med* 2009, **62**(6):1523-1532.

72. Edelman RR, Sheehan JJ, Dunkle E, Schindler N, Carr J, Koktzoglou I: **Quiescent-interval single-shot unenhanced magnetic resonance angiography of peripheral vascular disease: Technical considerations and clinical feasibility**. *Magn Reson Med*, **63**(4):951-958.

73. Storey P, Atanasova IP, Lim RP, Xu J, Kim D, Chen Q, Lee VS: **Tailoring the flow sensitivity of fast spin-echo sequences for noncontrast peripheral MR angiography**. *Magn Reson Med*, **64**(4):1098-1108.

74. Atanasova ISP, Lim R, Xu J, Chen Q, Laine A, Lee VS: **Effect of flip angle evolution on flow sensitivities in ECG-gated fast spin echo MRA methods at 3T**. *Proc Intl Soc Mag Reson Med* 2009:3903.

75. Haneder S, Attenberger UI, Riffel P, Henzler T, Schoenberg SO, Michaely HJ: **Magnetic resonance angiography (MRA) of the calf station at 3.0 T: intraindividual comparison of non-enhanced ECG-gated flow-dependent MRA, continuous table movement MRA and time-resolved MRA**. *European radiology* 2011, **21**(7):1452-1461.

76. Greenman RL, Shirosky JE, Mulkern RV, Rofsky NM: **Double inversion black-blood fast spin-echo imaging of the human heart: a comparison between 1.5T and 3.0T**. *J Magn Reson Imaging* 2003, **17**(6):648-655.

77. Storey P, Lim RP, Kim S, Stoffel DR, Lee VS: **Arterial flow characteristics in the presence of vascular disease and implications for fast spin echo-based noncontrast MR angiography**. *J Magn Reson Imaging*, **34**(6):1472-1479.

78. Li G, Sauerbier, C. , Paul, D. , Zhang, W. , He, Q. , Beckmann, M. , Lauer, L.: **Verse-SPACE**. *Proc Intl Soc Mag Reson Med 18* 2010:3036.

79. Atanasova IP, Storey P, Kim D, Lim RP, Lee VS: **ECG-gated fast spin echo MRA with interleaved acquisition of systolic and diastolic data for improved robustness to motion**. *Proc Intl Soc Mag Reson Med* 2012:1272.

80. Atanasova IP, Kim D, Storey P, Rosenkrantz A, Lim RP, Lee VS: **Sagittal Fresh Blood Imaging with Interleaved Acquisition of Systolic and Diastolic Data for Improved Robustness to Motion**. *Magn Reson Med* 2013 (In Press).

81. Hodnett PA, Koktzoglou I, Davarpanah AH, Scanlon TG, Collins JD, Sheehan JJ, Dunkle EE, Gupta N, Carr JC, Edelman RR: **Evaluation of peripheral arterial disease with nonenhanced quiescent-interval single-shot MR angiography**. *Radiology* 2011, **260**(1):282-293.

82. Hodnett PA, Ward EV, Davarpanah AH, Scanlon TG, Collins JD, Glielmi CB, Bi X, Koktzoglou I, Gupta N, Carr JC *et al*: **Peripheral arterial disease in a symptomatic diabetic population: prospective comparison of rapid unenhanced MR angiography (MRA) with contrast-enhanced MRA**. *AJR American journal of roentgenology* 2011, **197**(6):1466-1473.